Hypoplastic constitutive models for frozen soil

A dissertation for the doctor's degree submitted to
University of Natural Resources and Life Sciences, Vienna

Submitted by

Guofang Xu, MSc

Under the supervision of
Univ. Prof. Dr.-Ing. Wei Wu
Institute of Geotechnical Engineering
Department of Civil Engineering and Natural Hazards

January 2014

謹以此文獻給我的母親!

Universität für Bodenkultur Wien
Institut für Geotechnik

Erklärung zur Dissertation

Ich, Guofang Xu, bestätige hiermit, dass ich die beiliegende Dissertation selbstständig verfasst habe. Ebenso bestätige ich, dass keine anderen als die angegebenen Quellen und Hilfsmittel benutzt wurden.

Wien, Januar 2014

Declaration of dissertation

I, Guofang Xu, hereby confirm, that I write the enclosed dissertation all by myself. I also confirm, that nothing more than the given sources and auxiliary materials are used.

Vienna, January 2014

Acknowledgment

This dissertation would not have been accomplished without the help, encouragement and patience of my principal supervisor, Univ. Prof. Dr.-Ing. Wei Wu, not to mention his advice and unsurpassed knowledge of constitutive modeling. The good advice, support and friendship of my second supervisor, Prof. Dr. Jilin Qi, have been invaluable on both an academic and a personal level, for which I am extremely grateful.

A special thanks to my family. Words cannot express how grateful I am to my mother and father for all the sacrifices that they have made on my behalf. I would also like to thank all my colleagues and friends who supported me in writing this dissertation.

Finally, I would like to thank the China Scholarship Council (CSC) and Fonds zur Förderung der Wissenschaftlichen Forschung (FWF) for the funding, which support my research work and life for three years.

Abstract

Constitutive modeling for frozen soil is an important topic in frozen soil mechanics and construction in permafrost regions. This study, with the help of hypoplasticity theory, presents three constitutive models for frozen soils. The first model, called extended hypoplastic constitutive model, is obtained by introducing a temperature-dependent cohesion tensor and a deformation-related scalar function into the pioneer model developed by Wu (1992). Then by simulating some triaxial compression tests at different temperatures and confining pressures, the extended model is shown to have a good ability in describing the strength behavior and volumetric change of frozen soil. However, this model is rate-independent and thus cannot account for the loading rate effect and rheological properties of frozen soil. In view of this, the second model, named as visco-hypoplastic constitutive model, is then developed. This viscous model is obtained by dividing the stress rate into a statical and a dynamical part, which are represented by the extended model and a high order model with respect to strain, respectively. Then the versatility of this viscous model is verified by simulating some compression tests at different loading rates and creep tests at different stress levels. The third model, termed hypoplastic creep model, is developed especially for the rheological properties of frozen soil. By simulating some compression creep tests, this creep model is also shown to be capable of describing the creep behaviors of frozen soil, *e.g.* the time to creep failure and the minimum creep rate in the secondary creep stage. Besides, the relaxation of creep strength of frozen soil can also be described by this creep model.

Keywords: Frozen soil, Hypoplasticity, Constitutive Model, Rate-dependence, Rheological property

Zusammenfassung

Die Modellierung von Permafrost-Böden liefert wichtige Beiträge für die Bodenmechanik und die Bauwerke in Permafrost Regionen. In dieser Studie werden mit Hilfe der Hypoplastizitätstheorie drei Grundlagenmodelle für gefrorene Böden präsentiert. Das erste Modell, „ErweitertesHypoplasticConstitutive Model“ genannt, wurde, basierend auf dem Pionier-Modell von Wu (1992), durch Erweiterung um einen temperaturabhängigen Kohäsionstensor sowie einer verformungsabhängigen Skalarfunktion entwickelt. Durch dreiaxiale Kompressionsversuche bei unterschiedlichen Temperaturen und unterschiedlichen Radialdrücken konnte gezeigt werden, dass sich dieseserweiterte Modell gut zur Beschreibung des Festigkeitsverhaltens und der Volumenänderungen von Permafrost-Böden eignet. Da bei diesem Modell die Belastungsgeschwindigkeit unberücksichtigt bleibt, ist es nicht möglich Belastungseffekte und ihre rheologischen Wirkungen für Permafrost-Böden darzustellen. Aus diesem Grunde wurde ein zweites Modell entwickelt. Es wird als „Visco-HypoplasticConstitutive Model“ bezeichnet. Dieses viskose Modell wurde durch die Aufteilung der Spannungszunahmein einen statischen und einen dynamischen Teil gewonnen, bzw. durch ein einfaches und ein höher Grade Numerische-Modellzur Berücksichtigung der Spannungsbeschleunigung. Die Gültigkeitdieses viskosen Modells wurde durch Kompressionsversuche mit unterschiedlichenBelastungsraten, und mehrere Kriechversuchen geprüft. Das dritte Modell, als „HypoplasticCreep Modell“ bezeichnet, wurde speziell für die Simulation der rheologischen Eigenschaften von Permafrost-Böden entwickelt. Anhand von Druck-Kriechversuchen konnte gezeigt werden, dass dieses Modell ebenso zur Beschreibung des Kriechverhaltens von Permafrost-Böden, wiez.B. der Zeit bis zum Kriechversagen und der minimalen Kriechrate im sekundären Kriechen,geeignet ist. Außerdem kann auch die Spannungsrelaxation von Permafrost-Böden in diesem

Modell bestimmtwerden.

Schlagworte: Permafrostböden, Hypoplastizität, Geschwindigkeitsabhängig-Stoffmodell, rheologischeBodeneigenschaft

Contents

1 Introduction

1.1 Statement of problems

In the past century, a large number of engineering activities have been conducted in permafrost regions over the world. For example, Trans-Siberian Railway and Qinghai-Tibet Railway, oil pipelines in northwestern Canada and in northeastern China, Whittier tunnel in north America and Feng-huo-shan tunnel in western China, Bering Strait Crossing planned to connect Siberia with Alaska, and so on. During the construction and operation of these projects, the weight of the structure and various loads will be transmitted to frozen subsoil (or frozen ground) through foundations, so the bearing capacity and deformation of the frozen subsoil should be taken into consideration, which is important to the successful construction and safe running.

From elasticity we know that the equations of motion and continuity, which describe the equilibrium and compatible deformation of an element respectively, have nothing to do with the material *per se*. The main task in the assessment of the stability of frozen ground is to set up an appropriate constitutive equation (constitutive model) which can describe the stress-strain-time relationship for frozen soil. Therefore, study of constitutive modeling for frozen soils has become an important topic in frozen soil mechanics, which has not only practical value for the construction and maintenance of engineering in permafrost regions, but also important scientific significance in developing and perfecting frozen soil mechanics.

1.2 Constitutive models for frozen soils

In this section, plenty of constitutive models for frozen soils are reviewed. Basically, these models can be classified into 2 types: rate-independent and rate-dependent. The rate-independent models are developed with the main purpose of describing the stress-strain relationship of frozen soil at different test conditions, as will be discussed

in Subsection 1.2.1, while the rate-dependent models, besides the same function as the rate-independent models, are expected to be able to account for the effect of loading-unloading rate and rheological behaviors of frozen soil. However, owing to the complexity of the mechanical properties of frozen soil, progress is made mainly in a branch of rate-dependent models, namely creep constitutive models, which will be talked in Subsection 1.2.2.

1.2.1 Constitutive models with respect to stress-strain behavior

A special geomaterial, frozen soil contains ice and unfrozen water which could lead to rather complicated mechanical behaviors and bring many difficulties in modeling. Nevertheless, constitutive modeling has been a hot spot and attracted intensive attention from researchers during the past 40 years. Most of the existing constitutive models in this subsection have been developed based on two different viewpoints: macro-phenomenological and micro-mechanistic. The former type is obtained based on some macroscopic experimental observations at different test conditions, while the latter type deals with properties at a micro level, *e.g.* molecule or particle level, and provides knowledge of mechanism that controls macroscopic mechanical behavior of frozen soil. It is noteworthy that both the two types can be essentially regarded as an extension of the theory of plasticity by combining the effect of temperature of frozen soil, even though the latter type is titled micro model.

Typical examples of the macro-phenomenological models can be found as: under small deformation assumption, Cai *et al*. (1990) decomposed the total strain rate into viscoelastic strain rate and plastic strain rate, then proposed a visco-elastoplastic constitutive model for frozen soil, which is suitable for monotonic loading and cyclic loading; Rong *et al*. (2005) proposed 2 formulas for calculating Green stress and Kirchhoff stress, and developed a constitutive model for frozen soils under finite deformation; based on the result of triaxial compression tests on frozen Qinghai-Tibet sandy soil, Lai *et al*. (2009) obtained plastic potential and failure surface with the help of orthogonal flow rule, and then proposed an elastoplastic constitutive model for frozen sand. It should be mentioned that these models were obtained by analogizing

the constitutive models for unfrozen soils within the framework of elastoplasticity, more detailed information on these elastoplastic models will be presented in Subsection 1.2.3.

In addition to the macroscopic models talked above, efforts were also made in the development of micro-mechanistic constitutive models. Based on continuum mechanics and thermodynamics, He *et al*. (1999) proposed a damage constitutive model for frozen soil, in which a damage threshold was determined and dissipation potential function was established; Ning and Zhu (2007) built a relationship between the elastic constants of soil, water and ice and that of frozen soil mass based on mesomechanics of composite materials. Then a constitutive model was developed, which could consider the evolution of damage. It is undeniable that these models indeed have some advantages in mechanism explanation of the macroscopic behavior of frozen soil. However, how to properly evolve the damage factor poses a great challenge to the investigators.

1.2.2 Constitutive models with respect to creep behavior

As is known to all, creep is one of the most important mechanical properties of frozen soil, which may cause instability of infrastructures, such as roadbed, tunnel, etc. and natural disasters, *e.g.* landslide and debris flow, in permafrost regions. Following the creep theories for unfrozen soils and metals, large progress is also made in creep models for frozen soils upon the results of creep tests at different stress conditions. Based on the aging theory developed for the creep of metals, the following power relationship was proposed by Vyalov *et al*. (1962) to describe the creep process of frozen soil at constant temperature

$$A_0 \cdot \varepsilon^m = \alpha \cdot t^{\alpha} \tag{1.1}$$

in which A_0, m and α are parameters, t is time. It is found that the above model is only valid for the deformation before the tertiary creep stage, especially for a primary creep stage dominated process. Besides, the model is not suitable for the case with large variation of creep stress.

By introducing the method proposed by Hult (1966) for the creep of metals,

Ladanyi (1972) developed a secondary creep theory for frozen soils, with the purpose of using the theory to calculate the bearing capacity of buried footings and anchors. The secondary creep theory by Ladanyi (1972) has the following form

$$\varepsilon = \varepsilon_k [\frac{\sigma}{\sigma_k(T)}]^k + \dot{\varepsilon}_c [\frac{\sigma}{\sigma_c(T)}]^n \cdot t \tag{1.2}$$

where ε_k is an arbitrary small standard strain unit introduced only for convenience in calculation and plotting of data, $\dot{\varepsilon}_c$ is a small arbitrary standard stain rate rendering the model a normalized form, σ_k, σ_c, k and n are creep parameters, T is temperature. It should be noted that this theory is obtained by approximating the creep strain curve in the unsteady primary creep stage by a straight line which has the same slope as that in the steady secondary creep stage. This signifies that the theory can only account for creep process at moderate creep stress when the secondary creep stage is dominant.

In order to describe the complete three-stage creep process, unified models were studied by Assur (1980) and Fish (1982), which can be expressed as

$$\dot{\varepsilon} = (\dot{\varepsilon}_m / e^{\beta})(t_m / t)^{\beta} \exp(\beta t / t_m) \tag{1.3}$$

in which t_m is the time to creep failure, $\dot{\varepsilon}_m$ is the minimum creep strain rate, β is a creep parameter dependent on the temperature and water content of frozen soil. It is examined by Fish (1982) that creep behaviors at different creep stresses can be described by the above model. However, as the time to failure is introduced as a known quantity, this model cannot predict the service life or long term stability of the structures in permafrost regions, which is also pointed out by Zhu and Carbee (1983).

Compared to model (1.3), a similar creep model which can also describe the three-stage creep process was proposed by Ting (1983). The model has the form of

$$\dot{\varepsilon} = A \cdot e^{\beta t} \cdot t^{-m} \tag{1.4}$$

in which A, β and m are parameters. Comparison with the primary and secondary creep models (see models (1.1) and (1.2)) indicates that the above model makes fairly accurate fits of strain (rate) - time behavior of frozen sand. However, this model can only be applied for loading conditions which are sufficient large to cause creep rupture.

Till now, the merits and demerits of each of the above creep models have been illustrated. Besides, these representative models can also be found to have the following common deficiencies: 1) the models are constructed by creep strain (rate) being an explicit function of natural time, if the time approaches infinity, the creep strain (rate) will also approach infinity. Obviously, this is in contradiction to the results of creep test; 2) the models are developed especially for creep, thus can only describe the creep behaviors of frozen soil, the other rheological properties, such as strength relaxation and the effect of loading-unloading rate, cannot be accounted for effectually.

1.2.3 Discussion on the existing constitutive models

In the above two subsections, the advantages and disadvantages of the listed constitutive models (including rate-independent and rate-dependent) for frozen soils have been analyzed. It is noteworthy that most of the models in Subsection 1.2.1 have a physical background of elasticity and plasticity theory, while the creep models in Subsection 1.2.2 are mainly based on data fitting, as can be seen from (1.1) - (1.4).

As is well known, elastoplasticity theory, especially plasticity theory, is developed originally from metallic materials. In general, an elastoplasticity-based model consists of two parts: elastic model and plastic model. To get an elastic model is not difficult, the main work is to determinate the elastic constants, for example, elastic modulus E and Poisson's ratio v. However, to get a plastic model is much more difficult, especially when the material is in a complex stress state, the main work of which includes: i) to define a yield criterion; ii) to describe a flow rule; and iii) to determine a hardening law. When dealing with these problems for granular materials, *e.g.* soil, it is much more difficult than dealing for metallic materials. For example, in problem i), the yield criterion for granular materials is more difficult to be determined, which is mainly because the yield point on the stress-strain curve of granular material is not as clear as that for metallic materials. Therefore, the yield criterion for granular material is often determined based on hypotheses or numerous tests under different stress paths (Li, 2004).

In order to solve the other two problems, *i.e.* determination of flow rule and hardening law, let us make a deeper view of the core of plasticity theory, *viz*. $\mathrm{d}\boldsymbol{\varepsilon}_{ij}^{\mathrm{p}} = \Delta\lambda(\partial g / \partial \boldsymbol{\sigma}_{ij})$, in which g is a hypothetical function of plastic potential. In different constitutive models, plastic potential function could be determined with plastic strain increment obtained from many tests or with hypothesis-based method (Li, 2004), for some materials this potential function even does not exist. For problem ii), flow rule is used to determine the direction of plastic strain increment, which is stipulated, ponderously by plasticity, perpendicular to the plastic potential surface. This is to say, the determination of flow rule (an associated one) will boil down to the determination of plastic potential function, which is mainly based, as forementioned, on redundant tests or hypothesis. For problem iii), a material is said to be hardened, if the yield stress increases with the development of plastic deformation. In plasticity, hardening law describes the law of variation of yield criterion with the development of plastic deformation. Again, we encounter here the awful problem, yielding of granular materials, see problem i).

The above discussion has illustrated the elements of an elastoplastic constitutive model, from which we can see that excessive dependence on experiments or too many hypotheses are involved in model development. For example, the yield criterion and plastic potential function are determined based on hypothesis or experiments, as well as flow rule which is based on the latter. At this stage, we can conclude that it is cumbersome to model granular materials with elasticity and plasticity theory. When noting that the mechanical behavior of frozen soil is affected by more factors than that of normal granular materials, *e.g.* unfrozen soil, constitutive modeling would become more complicated if within the framework of plasticity theory. In light of this, new methods for material modeling can be resorted to.

1.3 Research method in this study

Hypoplasticity, a new theory developed with the help of continuum mechanics, has been becoming quite popular in the study of constitutive models for granular materials.

In hypoplasticity, constitutive model is built by stress rate being a tensor function of stress state and strain rate according to the representation theorem for isotropic tensor function. Compared to traditional elastoplasticity theory, hypoplasticity has many advantages in material modeling, such as: 1) the nonlinear stress-strain relationship from beginning to end based on hypoplastic model can coincide qualitatively with the characteristics of the deformation of granular materials; 2) failure surface and flow rule in hypoplasticity can be obtained rigorously in mathematics, rather than by assumption or experimental results as in elastoplasticity; 3) distinction between loading and unloading is not necessary to be made during numerical calculations, since the loading-unloading criterion is hidden in hypoplastic models *per se*; and 4) hypoplastic constitutive equations have a concise structure in mathematics.

In view of the above advantages of hypoplasticity, plenty of hypoplastic constitutive models (Kolymbas, 1985; Wu and Kolymbas, 1990; Wu, 1992; Wu and Bauer, 1994; Wu *et al*., 1996; Herle and Kolymbas, 2004; Huang *et al*., 2006; Zhang *et al*., 2008) are built for various geomaterials, from which hypoplasticity has been proved to be a powerful tool in describing all kinds of properties, such as nonlinear mechanical property, dependence on stress path, shear dilation and strain softening of geomaterials. So in this study, based on hypoplasticity theory, some constitutive models are developed for the special geomaterial - frozen soil.

1.4 Outline of the study

Constitutive modeling for frozen soil is the main topic of this study. Before proceeding to model, the necessity of modeling and the existing constitutive models for frozen soils are analyzed in Section 1. Then in Section 2, by introducing a cohesion tensor and a deformation function into the model developed by Wu (1992), an extended hypoplastic constitutive model for frozen soil is obtained. By simulating some triaxial compression tests at different temperatures and confining pressures, the model shows a good ability in describing the strength behavior and volumetric change of frozen soil. It should be noted that the model in Section 2 is rate-independent, thus

it cannot account for the loading rate effect and rheological properties of frozen soil. In view of this, a rate-dependent hypoplastic constitutive model, named as visco-hypoplastic constitutive model, is developed in Section 3. This viscous model is obtained by dividing the stress rate into a statical and a dynamical part, which are formulated by the rate-independent model in Section 2 and a high order model with respect to strain acceleration, respectively. Then the versatility of the viscous model is examined by simulating some compression tests at different loading rates and creep tests at different creep stresses. In Section 4, another rate-dependent hypoplastic constitutive model, termed hypoplastic creep model, is developed. By simulating some compression creep tests, this creep model is also shown to be capable of describing the creep behaviors, as well as relaxation of creep strength of frozen soil. In Section 5 the main conclusions of this study are listed, followed by some open questions and remarks on each model. The structure chart of this study is shown in Figure 1.1.

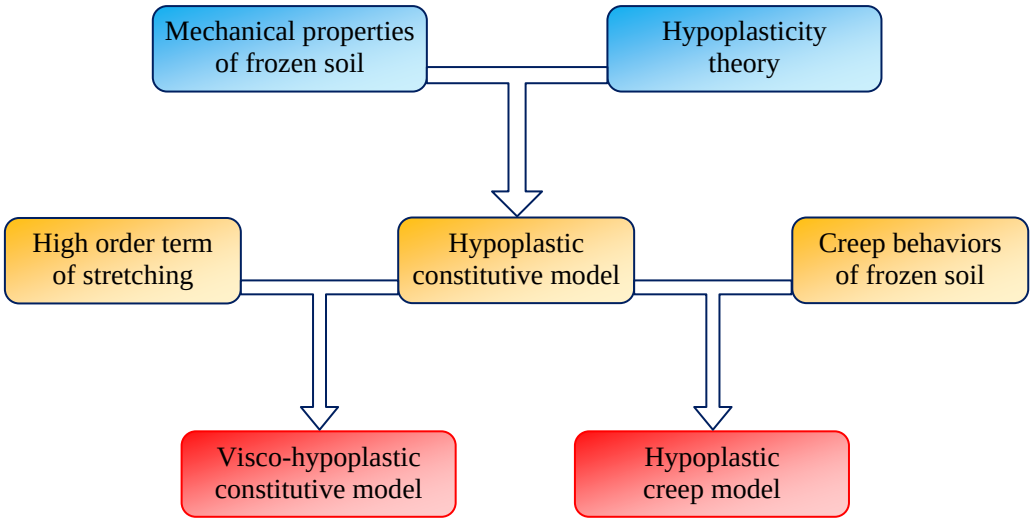

Fig. 1.1 Structure chart of the study

2 An extended hypoplastic constitutive model for frozen soil

At the beginning of this section, the theoretical background of hypoplasticity is briefly introduced. Then, by introducing a temperature-dependent cohesion tensor and a scalar function of deformation into the model developed by Wu (1992) for sand, an extended hypoplastic constitutive model for frozen soil is obtained. The method for determining the parameters in this model is also presented. Using the parameters determined with this method, the model is then verified by simulating some triaxial compression tests at different temperatures and confining pressures.

2.1 A brief introduction to hypoplasticity

Hypoplasticity is a new theory which is developed by many researchers (Kolymbas, 1985; Dafalias, 1986; Wu and Kolymbas, 1990; Wu, 1992) to study the constitutive models for granular materials. In hypoplasticity, the constitutive models are developed by means of the representation theorem for isotropic tensor function and have a theoretical basis of continuum mechanics. Generally, hypoplastic constitutive models are formulated by the stress rate being a nonlinear incremental function of stress and strain rate. When the nonlinear terms in the function are removed, the model will recover to a hypoelastic one (Truesdell, 1955).

Hypoplasticity has been widely used in material modeling, plenty of hypoplastic constitutive models have been proposed by many investigators (Wu and Bauer, 1994; Wu *et al*., 1996; Herle and Kolymbas, 2004; Zhang *et al*., 2008) for various granular materials, from which the advantages of hypoplasticity in modeling can be summarized as: 1) the deformation of granular materials is not decomposed factitiously into elastic and plastic part as in elastoplasticity. Hypoplasticity theory can describe the nonlinear deformation from the very beginning of loading, this seems more appropriate for granular materials, because the deformation of granular materials is mainly caused by the unrecoverable relative displacement between grains; 2) failure criterion, which can only be obtained from experiments or by assumption in

plasticity theory, can be derived directly from hypoplastic constitutive equation, which not only helps to circumvent the redundant experiments, but also has more significance from a mathematical point of view; 3) in hypoplasticity there is no concept of plastic potential which is assumed to exist to determine the flow rule in plasticity theory. So the flow rule in hypoplasticity is not obtained by perpendicularity to the plastic potential surface. Like failure criterion, flow rule can also be derived from hypoplastic constitutive equation; 4) loading-unloading criterion is not defined additionally as in plasticity theory, but incorporated implicitly in hypoplastic constitutive equations *per se*. This can greatly increase the efficiency of numerical simulations based on hypoplastic constitutive models; and 5) compared to elastoplastic constitutive equations, hypoplastic constitutive equations are more mathematically concise, also less experiments are required to determine the parameters in hypoplastic models.

2.2 Basic ideas of modeling frozen soil with hypoplasticity

For almost all the macroscopic constitutive models for frozen soils, they have a common basis which reads that the frozen soil is regarded as a homogeneous continuum, and the ice distributes uniformly in soil mass. This makes it possible to model frozen soils with hypoplasticity which is based on continuum mechanics. Secondly, many test results (Sayles, 1966; Ladanyi, 1981; Haynes and Karalius, 1977; Parameswaran, 1980; Bragg and Andersland, 1981) reveal that the factor which governs the mechanical properties of frozen soil is temperature. This can be attributed to the following 2 aspects: firstly, the mechanical properties of ice in frozen soil are strongly dependent on temperature; secondly, the bonding strength of the interface between soil grain and ice is also very sensitive to temperature. From this point of view, the strength of frozen soil can be regarded to consist of two parts, namely the strength of soil skeleton and ice cementation, see also Goughnour and Andersland (1968). Therefore, when the cementation of ice is taken into account, a hypoplastic constitutive model for frozen soil can be built based on the hypoplastic models for

cohesionless soil. The detailed procedures of modeling will be discussed in the next section.

2.3 Hypoplastic constitutive model for frozen soil

2.3.1 Framework of hypoplasticity

In the work by Wu and Kolymbas (1990), a general hypoplastic constitutive model was defined by assuming that there existed a tensor function **H** such that

$$\overset{\circ}{\mathbf{T}} = \mathbf{H}(\mathbf{T}, \mathbf{D}) \tag{2.1}$$

where **T** is stress tensor, **D** is stretching tensor, $\overset{\circ}{\mathbf{T}}$ is Jaumann stress rate and is defined as

$$\overset{\circ}{\mathbf{T}} = \dot{\mathbf{T}} + \mathbf{T}\cdot\mathbf{W} - \mathbf{W}\cdot\mathbf{T} \tag{2.2}$$

where **W** is a spin tensor.

In order to get a concrete model, constitutive equation (2.1) should be subjected to three restrictions. Two of these restrictions are based on general principles of continuum mechanics, while the other is based on experimental observations.

To start with a simple case, the constitutive model is considered to be rate-independent, *i.e.* the natural time should not appear in the constitutive equation. For constitutive equation (2.1), this is equivalent to:

Restriction 1: The function **H** should be positively homogeneous of the first degree in **D**

$$\mathbf{H}(\mathbf{T}, \lambda\mathbf{D}) = \lambda\mathbf{H}(\mathbf{T}, \mathbf{D}) \tag{2.3}$$

where λ is an arbitrary positive scalar.

The second restriction is based on the following experimental observation made by Goldscheider (1982) with a true triaxial apparatus on sand:

A proportional strain (stress) path starting from a nearly stress free and undistorted state yields a proportional stress (strain) path.

This observation is of fundamental importance for developing constitutive equations. Mathematically, it can be expressed by the following restriction.

Restriction 2: The function **H** should be homogeneous in **T**, *i.e.*

$$\mathbf{H}(\lambda\mathbf{T},\mathbf{D}) = \lambda^n \mathbf{H}(\mathbf{T},\mathbf{D}) \tag{2.4}$$

where λ is an arbitrary scalar and *n* denotes the degree of homogeneity. Restriction 2 implies that the tangential stiffness is proportional to the *n* th order of the stress level $(\mathrm{tr}\mathbf{T})^n$, so that experiments conducted under different stress levels can be normalized by $(\mathrm{tr}\mathbf{T})^n$.

The third restriction results from the requirement of objectivity of constitutive equation (2.1) under rigid rotations. For this requirement, it means

Restriction 3: The function **H** should fulfill the following condition of objectivity

$$\mathbf{H}(\boldsymbol{Q}\mathbf{T}\boldsymbol{Q}^{\mathrm{T}},\boldsymbol{Q}\mathbf{D}\boldsymbol{Q}^{\mathrm{T}}) = \boldsymbol{Q}\mathbf{H}(\mathbf{T},\mathbf{D})\boldsymbol{Q}^{\mathrm{T}} \tag{2.5}$$

in which $\boldsymbol{Q}$ is an orthogonal tensor. The requirement of objectivity could be satisfied when function **H** is chosen according to the representation theorem for isotropic tensor function. In the most general case, the representation theorem for a tensor function with two symmetric tensor variables can be written as (Wang, 1970)

$$\begin{aligned}\overset{\circ}{\mathbf{T}} = {} & \alpha_0\boldsymbol{\delta}_{ij} + \alpha_1\mathbf{T} + \alpha_2\mathbf{D} + \alpha_3\mathbf{T}^2 + \alpha_4\mathbf{D}^2 + \alpha_5(\mathbf{TD}+\mathbf{DT}) \\ & + \alpha_6(\mathbf{T}^2\mathbf{D}+\mathbf{DT}^2) + \alpha_7(\mathbf{TD}^2+\mathbf{D}^2\mathbf{T}) + \alpha_8(\mathbf{T}^2\mathbf{D}^2+\mathbf{D}^2\mathbf{T}^2)\end{aligned} \tag{2.6}$$

where δ_{ij} is Kronecker delta. The coefficient α_i (i = 0, 1, …, 8) are functions of the invariants and joint invariants of **T** and **D**.

2.3.2 Modeling frozen soil with hypoplasticity

Bearing in mind that constitutive equation (2.1) should be homogenous in stress **T**, and beginning with the simplest case in assuming that the tensor function is homogeneous of the first order in **T**, Wu (1992) proposed the following hypoplastic constitutive equation:

$$\overset{\circ}{\mathbf{T}} = c_1(\mathrm{tr}\mathbf{T})\mathbf{D} + c_2\frac{\mathrm{tr}(\mathbf{TD})}{\mathrm{tr}\mathbf{T}}\mathbf{T} + c_3\frac{\mathbf{T}^2}{\mathrm{tr}\mathbf{T}}\|\mathbf{D}\| + c_4\frac{\mathbf{T}_{\mathrm{d}}^2}{\mathrm{tr}\mathbf{T}}\|\mathbf{D}\| \tag{2.7}$$

where c_i (i = 1, …, 4) are dimensionless material parameters; $\|\mathbf{D}\| = \sqrt{\mathrm{tr}(\mathbf{D}^2)}$ stands

for the Euclidean norm of strain rate tensor; $\mathbf{T}_{\mathrm{d}}$ is the deviatoric stress tensor and can be defined by

$$\mathbf{T}_{\mathrm{d}} = \mathbf{T} - \tfrac{1}{3}(\mathrm{tr}\mathbf{T})\boldsymbol{\delta}_{ij} \tag{2.8}$$

Since the original model (2.7) is proposed for cohesionless soil, it should be mentioned that the limit surface of this model is a cone with its apex at the origin in the principal stress space. Therefore, constitutive equation such as (2.7) allows no tensile stress, and is obviously not appropriate for frozen soils which can sustain certain tension owing to ice cementation. However, this shortcoming can be removed by extending the constitutive equation with a back stress $\boldsymbol{s}$ related to the cohesion of frozen soil as

$$\overset{\circ}{\mathbf{T}} = \mathbf{H}(\mathbf{T}, \boldsymbol{s}, \mathbf{D}) \tag{2.9}$$

$\boldsymbol{s}$ is assumed to be a diagonal matrix of the rank of 3, and the elements on the principal diagonal are identical with each other, whose magnitude can be regarded as the cohesion of frozen soil. It is worth noting that different chemical or physical causes for cohesion give rise to different material behaviors, in this study, the cohesion is only related to the temperature of frozen soil, the effect of water content and other factors, such as the chemical properties of soil grain and cementation of the soluble salts in frozen soil, are not taken into account.

Enlightened by the work by Wu *et al*. (1996) on granular materials and Bauer and Wu (1995) on cohesive powders, the hypoplastic constitutive model for frozen soil can be constructed in the following way:

$$\dot{\mathbf{T}} = c_1[\mathrm{tr}(\mathbf{T}\text{-}\boldsymbol{s})]\mathbf{D} + c_2\frac{\mathrm{tr}[(\mathbf{T}\text{-}\boldsymbol{s})\mathbf{D}]}{\mathrm{tr}(\mathbf{T}\text{-}\boldsymbol{s})}(\mathbf{T}\text{-}\boldsymbol{s}) + f_{\varepsilon}\cdot\left[c_3(\mathbf{T}\text{-}\boldsymbol{s})^2 + c_4(\mathbf{T}\text{-}\boldsymbol{s})_{\mathrm{d}}^2\right]\frac{\|\mathbf{D}\|}{\mathrm{tr}(\mathbf{T}\text{-}\boldsymbol{s})} \tag{2.10}$$

in which f_{ε} is a deformation-related factor.

Experimental results on frozen Fairbanks silt by Haynes and Karalius (1977) and on frozen sand by Bourbonnais and Ladanyi (1985) show that the shear strength of frozen soils depends linearly on temperature when the temperature is not lower than -30 $^{\circ}$C. In light of this, we assume that the element of $\boldsymbol{s}$ can be related to temperature as

$$s = a \cdot \theta + b \tag{2.11}$$

where θ is the temperature of frozen soil, a and b are parameters, which describe the effect of temperature on the cohesion of frozen soil.

The deformation-related factor is given by the following expression:

$$f_\varepsilon = 2 - \exp(\alpha \cdot l + \beta) \tag{2.12}$$

where α and β are parameters related to the existential state, such as temperature and stress state of frozen soil, l is the accumulation of deformation and can be obtained according to the definition in Wu *et al*. (1993).

2.3.3 Calibration of the hypoplastic constitutive model

Altogether there are 8 parameters to be determined in the extended constitutive model. These parameters can be classified into 2 groups: the first group comes from the original model (2.7), *i.e.* material parameters c_i (i = 1, …, 4), and the second group contains the other 4 parameters, a, b, α and β.

1. Determination of the material parameters

The material parameters in constitutive equation (2.7) can be determined from a conventional triaxial compression test. For the sake of convenience, the two linear terms and two nonlinear terms in (2.7) are abbreviated as $\mathbf{L}_1$, $\mathbf{L}_2$, $\mathbf{N}_1$ and $\mathbf{N}_2$, then equation (2.7) can be rewritten as

$$\dot{\mathbf{T}} = c_1\mathbf{L}_1(\mathbf{T}):\mathbf{D}+c_2\mathbf{L}_2(\mathbf{T}):\mathbf{D} + c_3\mathbf{N}_1(\mathbf{T})\|\mathbf{D}\| + c_4\mathbf{N}_2(\mathbf{T})\|\mathbf{D}\| \tag{2.13}$$

Owing to the symmetry of Cauchy stress tensor and strain tensor, equation (2.13) can be rewritten into the following two scalar equations

$$\dot{\mathrm{T}}_1 = c_1 L_{11}\mathrm{D}_1 + c_2 L_{12}\mathrm{D}_3 + c_3 N_{11}\sqrt{\mathrm{D}_1^2 + 2\mathrm{D}_3^2} + c_4 N_{12}\sqrt{\mathrm{D}_1^2 + 2\mathrm{D}_3^2} \tag{2.14}$$

$$\dot{\mathrm{T}}_3 = c_1 L_{21}\mathrm{D}_1 + c_2 L_{22}\mathrm{D}_3 + c_3 N_{21}\sqrt{\mathrm{D}_1^2 + 2\mathrm{D}_3^2} + c_4 N_{22}\sqrt{\mathrm{D}_1^2 + 2\mathrm{D}_3^2} \tag{2.15}$$

When the both sides of equations (2.14) and (2.15) are divided by axial strain rate, quantities such as stiffness and Poisson's ratio can be generated. To this stage, let us consider two arbitrary points A and B (in practice, the point at the outset of deviatoric stress and the failure point are preferred) on the stress-strain curve and the corresponding points A' and B' on the axial strain-radial strain curve, as shown in

Figure 2.1, from which the tangent modulus, $\boldsymbol{E}_A$ and $\boldsymbol{E}_B$, and Poisson's ratio, v_A and v_B, at the two points can be obtained. As the confining pressure is maintained constant during a triaxial compression test, we have $\dot{T}_2 = \dot{T}_3 = 0$ and $E_{3A} = E_{3B} = 0$ ($E_3 = \dot{T}_3 / D_3$). Substituting the relevant quantities at points A (A') and B (B') into equations (2.14) and (2.15), we can get

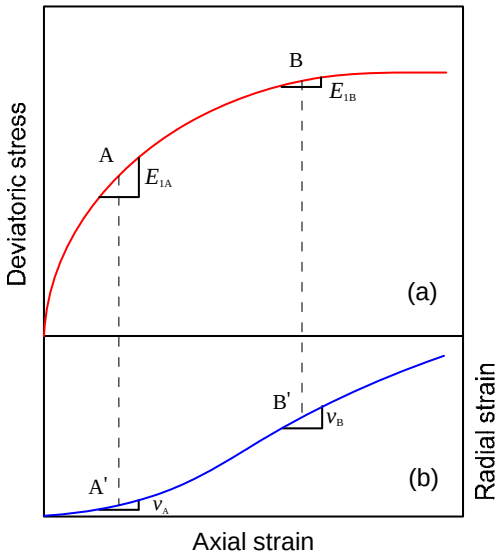

Fig. 2.1 Schematic curves of triaxial compression test

(a) deviatoric stress-axial strain; (b) radial strain-axial strain

$$E_{1A} = c_1 L_{11} + c_2 L_{12} v_A + c_3 N_{11} \sqrt{1+2v_A^2} + c_4 N_{12} \sqrt{1+2v_A^2} \tag{2.16}$$

$$0 = c_1 L_{21} + c_2 L_{22} v_A + c_3 N_{21} \sqrt{1+2v_A^2} + c_4 N_{22} \sqrt{1+2v_A^2} \tag{2.17}$$

$$E_{1B} = c_1 L_{11} + c_2 L_{12} v_B + c_3 N_{11} \sqrt{1+2v_B^2} + c_4 N_{12} \sqrt{1+2v_B^2} \tag{2.18}$$

$$0 = c_1 L_{21} + c_2 L_{22} v_B + c_3 N_{21} \sqrt{1+2v_B^2} + c_4 N_{22} \sqrt{1+2v_B^2} \tag{2.19}$$

Then the material parameters c_i (i = 1, …, 4) can be obtained by solving the above equation system with respect to the variables c_i.

If points A and B are chosen at the outset of deviatoric stress and the failure point, respectively, we can get the following information: 1) E_{1A} will be the initial tangent modulus of the specimen, *i.e.* E_i; 2) E_{1B} will be 0, then from (2.18) the stress ratio at

failure, $R_f = T_1/T_3$, can be obtained, which will generate the frictional angle at failure (φ) for cohesionless soil according to $\sin\varphi = (R_f - 1)/(R_f + 1)$; 3) v_A will be the initial Poisson's ratio (v_i) and v_B will be the Poisson's ratio at failure (v_f), each can be converted into the corresponding dilatancy angle ψ_i and ψ_f according to $\tan\psi = 1 + 2\cdot v$. Therefore it can be seen that the determination of the material parameters c_i can be replaced by the determination of the initial tangent modulus E_i, initial dilatancy angle ψ_i, frictional angle at failure φ and dilatancy angle at failure ψ_f, which are well defined in soil mechanics.

2. Determination of the introduced parameters

Here we proceed to determine the parameters in the second group, which contains 4 introduced parameters, a, b, α and β. As mentioned above, parameters a and b describe the dependence of cohesion on temperature, so a and b can be obtained from the relationship between cohesion and temperature (Figure 2.2). Parameter α is related to the configuration of stress-strain curve, *e.g.* strain softening or strain hardening; β is a coordination parameter. Considering that temperature is the most important factor which governs the mechanical behaviors of frozen soil, and for the sake of simplicity, α and β can be calculated with $\alpha = 1 - (\theta/\theta_{ref})^{n_1}$ and $\beta = -(\theta/\theta_{ref})^{n_2}$, respectively. θ_{ref} is a reference temperature which is used frequently in frozen soil mechanics, normally θ_{ref} has the value of -1 $^{\circ}$C (Zhu and Carbee, 1984). When different confining pressures are considered, θ in the above expressions for calculating α and β can be replaced by mean pressure p, then p_{ref} could be regarded as the pre-consolidation pressure p_c.

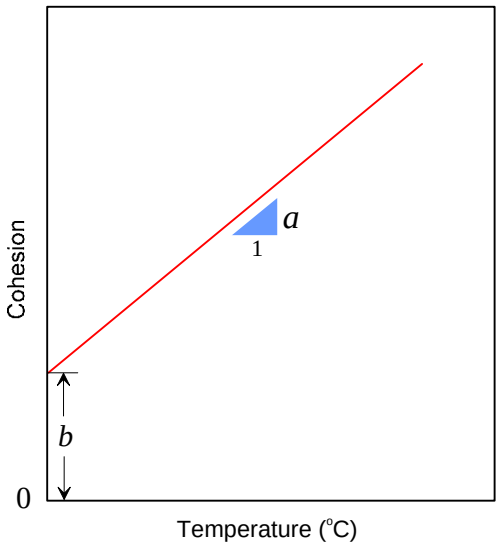

Fig. 2.2 Determination of parameters *a* and *b*

2.4 Verification of the hypoplastic constitutive model

To this stage, the constitutive model has been formulated and the calibration method has been determined, the ensuing question is to check whether this model is capable of describing the main mechanical properties, such as strength and deformation behaviors of frozen soil. For this purpose, several kinds of laboratory tests have been simulated. Owing to the simultaneous control of temperature and pressure is a big challenge when conducting experiments on frozen soil, comparisons between numerical and experimental results are only made based on conventional triaxial compression test, by means of which the simulation procedures are also presented.

2.4.1 Laboratory triaxial compression test

Specimen preparation

A standard sand is used in the compression tests. The maximum and minimum diameters of the sand are 2.0 mm and 0.075 mm, respectively. The half-content diameter d_{50} is 0.7 mm. The procedure of specimen preparation can be summarized as: firstly, the dry specimens are prepared with a so-called sand pluviation method (the sand flows through a nozzle and a series of sieves into a cylindrical mold of 61.8 mm in inner-diameter) which could guarantee a relatively uniform bulk density, proved by

Stetzler-Kaufmann (1983); secondly, sufficient distilled water is provided to be sucked by the dry specimen placed in a closed vacuum container; then the specimens are frozen quickly to avoid ice lens in a chamber at the temperature of -30 $^{\circ}$C. Such prepared specimen has a dry unit weight of 18.2 kN/m^3, and the dimensions of the specimen are 61.8 mm in diameter and 125.0 mm in height.

Test procedures

All the triaxial compression tests are conducted on a self-developed test apparatus, which consists of the following 4 parts: axial loading system, radial loading system, cooling system and data acquisition system. The detailed procedures of conducting a compression test on frozen soil specimen are listed in below:

i) *pre-cooling*. Before testing, the loading cap, pedestal, especially the oil which is used to control the temperature and confining pressure should be kept at a minus temperature required by the test, this could guarantee that the specimen would not melt when installing it;

ii) *installing specimen*. When pre-cooling is finished, the specimen will be taken out from the mold and packed into a rubber membrane, then installed quickly into the chamber of the test machine. Afterwards the chamber will be sealed and covered with an insulation shield. With the help of cooling system, the temperature of the oil will be maintained at the target value for at least 24 h;

iii) *loading process*. When the temperatures around the specimen are stable, a hydrostatic pressure of the magnitude of target confining pressure is firstly applied to the specimen and kept unchanged, then an axial pressure (deviatoric stress) will be applied by a vertical piston with a loading rate of 1.25 mm/min. During the whole loading process, the axial stress, axial deformation and radial deformation will be recorded automatically by the data acquisition system;

iv) *removing specimen*. When the test is finished, the confining oil will be recycled, then the specimen will be taken out and the characteristics of deformation and failure will be documented.

According to the above test procedures, some triaxial compression tests on

frozen soil at different test conditions are conducted, the test results will be presented in the next subsection together with the simulations based on the extended constitutive model.

2.4.2 Simulation of triaxial compression test

In this subsection, the extended hypoplastic constitutive model is used to simulate some triaxial compression tests at different temperatures and confining pressures, then the simulated results are compared to the test results in two aspects, namely stress-strain relationship and volumetric deformation.

Based on the extended model (2.10), the governing differential equations for a conventional triaxial compression test can be expressed as:

$$\dot{T}_1 = c_1[(T_1 - s_1) + 2(T_3 - s_3)]D_1 + c_2 \frac{(T_1 - s_1)D_1 + 2(T_3 - s_3)D_3}{(T_1 - s_1) + 2(T_3 - s_3)}(T_1 - s_1) + [c_3(T_1 - s_1)^2 + \frac{4}{9}c_4(T_1 - T_3)^2] f_\varepsilon \frac{\sqrt{D_1^2 + 2D_3^2}}{(T_1 - s_1) + 2(T_3 - s_3)} \quad (2.20)$$

$$\dot{T}_3 = c_1[(T_1 - s_1) + 2(T_3 - s_3)]D_3 + c_2 \frac{(T_1 - s_1)D_1 + 2(T_3 - s_3)D_3}{(T_1 - s_1) + 2(T_3 - s_3)}(T_3 - s_3) + [c_3(T_3 - s_3)^2 + \frac{1}{9}c_4(T_1 - T_3)^2] f_\varepsilon \frac{\sqrt{D_1^2 + 2D_3^2}}{(T_1 - s_1) + 2(T_3 - s_3)} \quad (2.21)$$

In the above two equations, the back stress s can be determined based on equation (2.11), and factor f_ε can be calculated according to equation (2.12) by setting $l = 0$ at the beginning of the test. Recalling the boundary conditions for a conventional triaxial compression test, *i.e.* 1) starting from a hydrostatic stress state $\mathbf{T}_0$; 2) keeping the confining pressure unchanged ($\dot{T}_3 = 0$); and 3) compressing at a constant axial strain rate, *e.g.* D_1 = -0.0001 (note that negative sign denotes compression and any positive scalar can serve as the norm of strain rate tensor, since the constitutive equation in concern is rate-independent.), equations (2.20) and (2.21) contain only two unknowns, *i.e.* $\dot{T}_1$ and D_3. Therefore the procedures of the simulation can be presented as: i) in each time step of the simulation, the radial strain rate D_3 is to be calculated from equation (2.21); ii) the radial strain rate (increment) obtained in this way will be substituted into equation (2.20) to get the axial stress rate (increment); and iii) the stress state will be updated to serve as the initial stress state for the simulation in the next time step.

Simulating the effect of temperature

A series of triaxial compression tests are conducted on frozen soil at a constant confining pressure (1.0 MPa) and constant strain rate (1.67×10^{-4} s^{-1}), however at different temperatures, which are -1, -2, -5 and -10 °C. Before the simulation of these tests, the parameters in the extended model should be determined. According to the stress-strain curve and volumetric deformation curve of the corresponding unfrozen standard sand, the required quantities for determination of the material parameters are obtained as: the initial tangent modulus E_i = 201.4 MPa, the initial dilatancy angle ψ_i = -43.0°, the frictional angle φ = 33.0° and dilatancy angle at failure ψ_f = 37°. Based on these quantities, the material parameters can be calculated as c_1 = -64.5, c_2 = -715.7, c_3 = -647.2, c_4 = 1483.0. Besides, based on the cohesion-temperature relationship, the introduced parameters can be obtained as: a = 481.0 kPa/°C, b = 1124.0 kPa, n_1 = 0.213, n_2 = -1.57. With these parameters and the simulation procedures listed above, the triaxial tests at the 4 different temperatures are simulated. The results are shown in Figures 2.3-2.4 together with the corresponding experimental results.

It can be seen from the results that, with the decrease of temperature, the strength and the initial tangent modulus of the frozen soil will increase. This is quite easy to be understood, for the structure of the frozen soil is enhanced by the increasing cementation of ice. Meanwhile, the axial strain at failure has a tendency to decrease. This could be explained by the change of phase from a plastic to a brittle type with the decrease of soil temperature. Comparison between the simulated and experimental results shows that the above behaviors can be well captured by the proposed model. For volumetric deformation, it is always a difficult problem to predict. The results of a workshop on constitutive models reveal that none of 32 models can get a score higher than 40 out of a full mark 100 in predicting volumetric deformation. With the proposed model, the simulated volumetric deformation is shown in Figure 2.4, from which we can see that the predictions and experimental results agree with each other to a large extent. To this stage, we could conclude that the proposed model shows a good ability in describing the effect of temperature on the main mechanical behaviors of frozen soil.

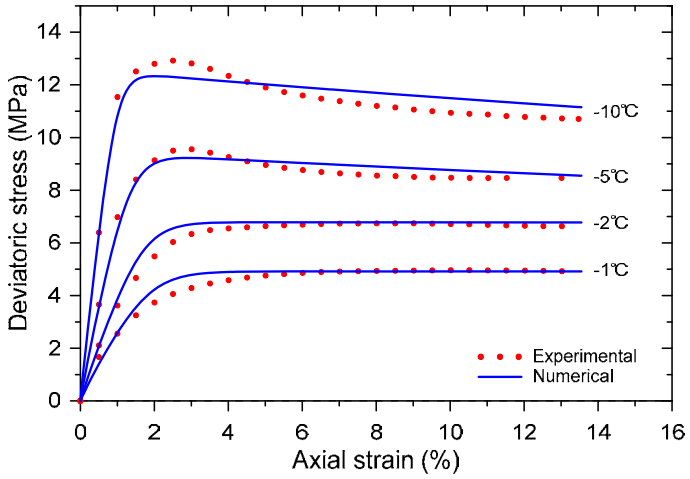

Fig. 2.3 Stress-strain relationship at different temperatures

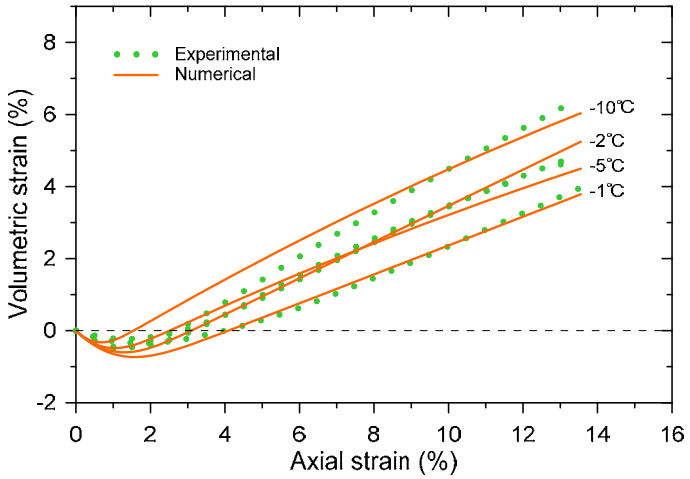

Fig. 2.4 Volumetric deformation at different temperatures

Simulating the effect of confining pressure

Triaxial compression tests at different confining pressures (0.3, 0.6, 0.8 and 1.0 MPa) are also simulated. The tests are conducted at the temperatures of -4.0 and -6.0 $^{\circ}$C and strain rate of 1.67×10^{-4} s^{-1}. The simulation results are presented in Figures 2.5-2.8. From Figures 2.5 and 2.7 we can see: i) both the strength and axial strain at failure increase with the increase of confining pressure; ii) the degree of strain softening tends to decrease as the confining pressure increases. The first observation is not difficult to understand, while for the second observation, it can be analogized to the results of triaxial tests on over-consolidated and normally consolidated soil in conventional soil mechanics. A soil can be regarded as an over-consolidated soil when

the present pressure on the soil is less than the pre-consolidation pressure in history, otherwise, it will be called normally consolidated soil. Keeping this in mind, when the confining pressure increases in triaxial tests, the test soil can be considered to change from an over-consolidated state to a normally consolidated state, therefore the degree of strain softening will decrease, as the over-consolidated soil is more apt to exhibit strain softening in stress-strain curve. By comparing the simulated results with the experimental results, we can find that the above observations can be well reproduced by the extended constitutive model.

The volumetric deformations of the specimens at the two temperatures are shown in Figures 2.6 and 2.8. From each figure we can see that the frozen soil specimen dilates at all confining pressures, the lower the confinement is, the stronger the dilation will be. Comparison between the numerical and experimental results indicates that the extended model is also capable of describing the characteristic of deformation at different confining pressures.

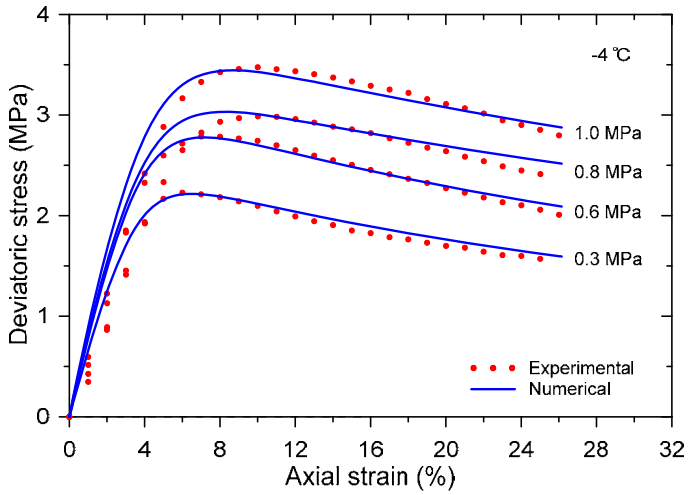

Fig. 2.5 Stress-strain relationship at different confinements at -4.0 ˚C

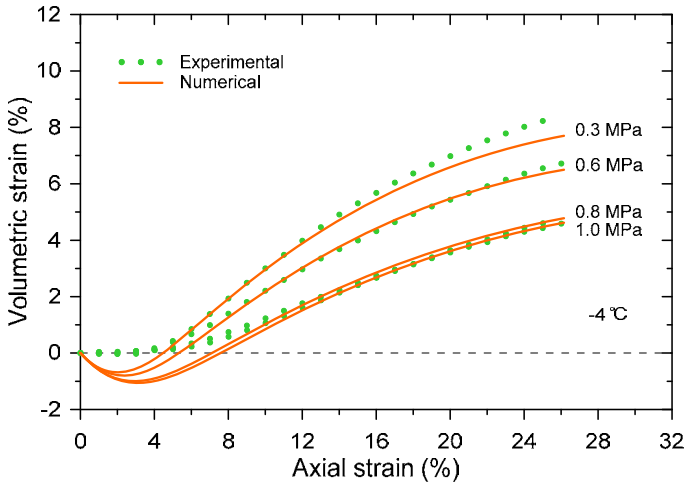

Fig. 2.6 Volumetric deformation at different confinements at -4.0 ˚C

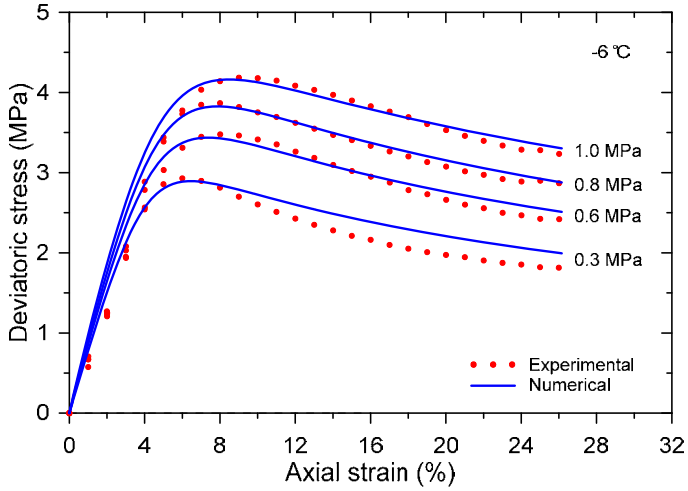

Fig. 2.7 Stress-strain relationship at different confinements at -6.0 ˚C

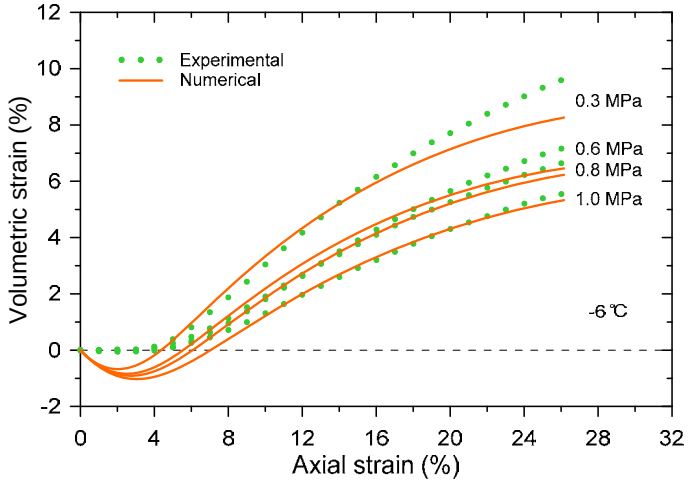

Fig. 2.8 Volumetric deformation at different confinements at -6.0 ˚C

2.5 Summary

In this section, an extended hypoplastic constitutive model for frozen soil is proposed based on the pioneer model by Wu (1992) and some novel ideas on the constitution of the strength of frozen soil. Then, a series of triaxial compression tests on frozen soils at different temperatures and confinements are simulated with this model. Comparisons between the simulated and experimental results show that the main mechanical behaviors of frozen soil, such as strength, axial strain at failure, strain softening and volumetric deformation, can be well captured by the extended model.

It should be noted that the model proposed in this section is rate-independent, thus it cannot account for the rheological properties of frozen soil, such as creep behaviors and loading rate effect, which are actually quite important in practical engineering. In view of this, a rate-dependent hypoplastic constitutive model for frozen soil will be presented in the next section.

3 A visco-hypoplastic constitutive models for frozen soil

A sound hypoplastic constitutive model was developed in Section 2, which can describe the main mechanical behaviors of frozen soils, such as the variation laws of strength and volumetric deformation with temperature and confining pressure. Admittedly, this model cannot account for time effect, *i.e.* rheological or viscous properties of frozen soil, thus should be attributed to rate-independent constitutive model.

In frozen soil engineering, the loading pattern on structures has become more and more complicated with the function richening and scale increasing of structures. In order to insure the serviceability of the structures, it is necessary to get a deep understanding of the effect of loading pattern, including loading rate, on the mechanical properties of the surrounding frozen soils. This is to say, the rheological property of frozen soils and rate-effect cannot be ignored, thus study on the stress-strain-time relationship of frozen soil, such as creep, relaxation and loading rate effect, etc. has become more and more important. Keeping these in mind, this section is planned to develop a rate-dependent hypoplastic constitutive model, also named here as visco-hypoplastic constitutive model, for frozen soil.

3.1 Development of the visco-hypoplastic constitutive model

The hypoplastic constitutive model in the last section is meant primarily to describe, we say, the *statical behaviors* of frozen soil, in which the dominating mechanism is friction. However, the same frozen soil may exhibit dynamical or fluid-like behaviors under certain condition, in which rate-effect and viscosity would be the major characteristics. Such behaviors are of great importance in numerous engineering problems. For example, in slope engineering in permafrost regions, many slopes exhibit gravity-driven creep movements as a result of the viscous behavior of frozen soil. Not only do these movements pose a threat to infrastructure and buildings on or below the slope, they may also represent an initial stage of fast landslides or earth

flows with even more detrimental impact. In road engineering, the deformation of roadbed can be caused not only by the thaw settlement of frozen subsoil, creep of the subsoil is also found to be an important cause of the deformation (Qi *et al*., 2007). In mining engineering, the mining procedure can be described as a continuous unloading process with the increase of mining depth, the unloading rate is directly dependent on the mining speed, which has a strong effect on the deformation and stability of the surrounding frozen soil. And in caving or tunneling engineering under frozen ground, excavation is also a complicated unloading process like in mining engineering, moreover, the deformation of frozen soil wall is confined by support, which can affect stress redistribution and then support duration. Therefore, when conducting such engineering activities in which the viscous behaviour or rate-effect cannot be neglected, it is necessary to develop a viscous constitutive model for frozen soil.

3.1.1 Conception of the structure of the viscous model

It is widely known that many liquids (including water) will briefly react like elastic solids when subjected to sudden stress, and conversely, many solids (even granite) will flow like liquids, albeit very slowly, even under arbitrarily small stress (Kumagai *et al*., 1978). Traditionally, the description of the fluid-like behavior of materials has been made independently from the theories for the solid-like behavior. One of the simplest cases, Newtonian fluid, is easy to be associated with for this description, which has the following form

$$\mathbf{T} = \eta\mathbf{D} \tag{3.1}$$

where **T** is Cauchy stress tensor, **D** is stretching tensor, η is the viscosity coefficient. However, Newtonian models within the framework of (3.1) cannot exhibit all normal stress differences (Meissner *et al*., 1989; Goldhirsch and Sela, 1996) in a simple shear flow, which would be the cause of Weissenberg effect.

In the later mechanical theories for the flow of liquid, especially flow of granular materials (Goodman and Cowin, 1971, 1972; Savage, 1979; Nunziato *et al*., 1980; Passman *et al*., 1980), the Cauchy stress **T** is of the form

$$\mathbf{T} = \boldsymbol{f}(v,\ \text{grad}\ v,\ \mathbf{D}) \tag{3.2}$$

where v is the grain volume fraction. It is not physically clear why the stress should depend on the gradients of v, however, some clues can be found in Savage (1979). It should be noted that models of the form (3.2) also have some limitations, they can only be applied to slow to moderately fast flows of dense granular materials. A detailed discussion of models of the class (3.2) can be found in the work by Massoudi (1991).

Incidentally, the complete representation theorem for the isotropic function of stress given by (3.2) should be of the following form

$$\mathbf{T} = a_0\mathbf{I} + a_1\mathbf{D} + a_2\mathbf{D}^2 + a_3 \operatorname{grad} v \otimes \operatorname{grad} v + a_4 \operatorname{sym} (\operatorname{grad} v\, (\mathbf{D} \otimes \operatorname{grad} v)) + a_5 \operatorname{sym} (\operatorname{grad} v\, (\mathbf{D}^2 \otimes \operatorname{grad} v)) \tag{3.3}$$

where the coefficients $a_0, a_1, \ldots, a_5$ are functions of

$$a_i = f\,(v; I_{\boldsymbol{D}}; II_{\boldsymbol{D}}; III_{\boldsymbol{D}}; \operatorname{grad} v \cdot \operatorname{grad} v, \operatorname{grad} v \cdot \boldsymbol{D} \operatorname{grad} v; \operatorname{grad} v \cdot \boldsymbol{D}^2 \operatorname{grad} v) \tag{3.4}$$

with the principal invariants

$$I_{\boldsymbol{D}} = \operatorname{tr}\mathbf{D};\ II_{\boldsymbol{D}} = \tfrac{1}{2}((\operatorname{tr}\mathbf{D})^2 - \operatorname{tr}(\mathbf{D}^2)),\ III_{\boldsymbol{D}} = \det\mathbf{D} \tag{3.5}$$

However, this representation theorem does not help very much in building constitutive models owing to its excessive complexity. As a consequence, most the early models are based on a part of the representation theorem, which is found to be the generalization of Reiner-Rivlin fluid model, and have the structure

$$\mathbf{T} = \alpha_0\mathbf{I} + \alpha_1\mathbf{D} + \alpha_2\mathbf{D}^2 \tag{3.6}$$

The coefficients α_i (i = 0, 1, 2) are functions of the principal invariants of **D** and grain volume fraction. However, these models are fraught with internal inconsistency, which has been succinctly discussed by Scheiwiller and Hutter (1982). Like the Newtonian fluid models, models within the framework of (3.6) can neither explain the normal stress effect.

Hitherto, it can be found without any difficulty that all the above models are based on a relationship between stress and strain rate. Besides the deficiencies of their own, such models cannot account for the different behaviors for loading and unloading, which therefore requires constitutive models to be formulated in a relatively complicated form, *e.g.* containing the rate form of stress or high order

derivatives of strain.

Before we proceed, let us consider some flow patterns in different materials. If the flow properties of a material can be completely characterized by a single variable viscosity coefficient, *e.g.* Newtonian flow, then the flow mode of the material under any different conditions can be worked out without difficulties in principle. For more complicated flows of materials which possess elasticity of volume or of shape to guarantee finite rate of shear (Fröhlich and Sack, 1946), they will exhibit properties at any instant which depend on their recent rheological history in the sense that the stress is not entirely determined by the instantaneous rate of strain. One of these flows is Maxwell flow (Maxwell, 1867), in which an additional rate of shear is proportional to the rate of application of stress $\dot{\mathbf{T}}$ at any instant, and the total rate of shear can be characterized with

$$\eta_0 \mathbf{D} = \mathbf{T} + \lambda_1 \dot{\mathbf{T}} \tag{3.7}$$

Here we can see that the hypoplastic constitutive model proposed in Section 2 has the same construction as Maxwell flow. Another flow was considered by Fröhlich and Sack (1946) on a system composed of a continuous and a disperse phase, the differential equation of flow for which was found to be of the form

$$\mathbf{T} + \lambda_1 \dot{\mathbf{T}} = \eta_0 (\mathbf{D} + \lambda_2 \dot{\mathbf{D}}) \tag{3.8}$$

in which λ_1 is the relaxation time, λ_2 is the retardation time. By comparing equations (3.7) and (3.8) we can see that the $\dot{\mathbf{D}}$ term in the second equation is comparable with the $\mathbf{D}$ term and cannot be neglected. In some cases, it is even necessary to consider higher time derivatives than the second derivative, for example in oscillatory shearing motion of small amplitude, then there being need to consider the equation of the following form:

$$\mathbf{T} + \lambda_1 \dot{\mathbf{T}} + \nu_1 \ddot{\mathbf{T}} + ... = \eta_0 (\mathbf{D} + \lambda_2 \dot{\mathbf{D}} + \nu_2 \ddot{\mathbf{D}} + ...) \tag{3.9}$$

where ν_1, ν_2,… are additional constants.

To this stage we can summarize the flow patterns of different materials as: 1) Maxwell flow can be considered as a flow with an additional shear rate proportional to the rate of application of stress on the basis of Newtonian flow; 2) when the strain

acceleration cannot be neglected, the flow studied by Fröhlich and Sack (1946) can be regarded as an extension of Maxwell flow. Enlightened by these conclusions, we can extend, following a similar approach, the hypoplastic constitutive model given in Section 2 to a viscous model, the details will be presented in below.

At first we assume that the stress and its rate can be decomposed into two parts, the first part for statical (rate-independent) behavior and the second part for dynamical (rate-dependent) behavior, *viz*.

$$\mathbf{T} = \hat{\mathbf{T}} + \check{\mathbf{T}} \qquad \mathring{\mathbf{T}} = \mathring{\hat{\mathbf{T}}} + \mathring{\check{\mathbf{T}}} \tag{3.10}$$

The statical part will be described by the constitutive equation (2.1) with minor modification. When rewritten out using $\hat{\mathbf{T}}$, it has the general form of

$$\mathring{\hat{\mathbf{T}}} = \hat{\mathbf{H}}(\hat{\mathbf{T}}, \mathbf{D}) \tag{3.11}$$

Compared to the statical part, the dynamical part is a little more difficult and will be talked separately in subsection 3.1.2, followed by the minor modification in the statical part in Subsection 3.1.3.

3.1.2 Dynamic part of the viscous model

In order to be accorded in form with the statical part (3.11) which is of rate type, the dynamical part has to be formulated in rate as well. To this end, let us consider the following equation which could be regarded in form as the time differentiation of Equation (3.1) provided the viscosity coefficient is a constant

$$\mathring{\check{\mathbf{T}}} = \eta \mathring{\mathbf{D}} \tag{3.12}$$

where $\mathring{\mathbf{D}}$ is the Jaumann stretching rate tensor and can be obtained according to the scheme in (2.2), that is

$$\mathring{\mathbf{D}} = \dot{\mathbf{D}} + \mathbf{D} \cdot \mathbf{W} - \mathbf{W} \cdot \mathbf{D} \tag{3.13}$$

The Jaumann stretching rate tensor can be compared to the Rivlin-Ericksen tensor (Rivlin and Ericksen, 1955; Truesdell and Noll, 1965), which is defined as the coefficients $\mathbf{A}_n$ in the Taylor series of the relative right Cauchy-Green strain tensor at $\tau = t$:

$$\mathbf{C}_t(\mathrm{x},\tau)=\sum_{n=0}\frac{(\tau-t)^n}{n!}\mathbf{A}_n(\mathrm{x},t) \tag{3.14}$$

where the tensor $\mathbf{C}_t(\mathrm{x},\tau)$ describes the deformation at time τ of the element which is at x at time *t*. A recursive relationship between the Rivlin-Ericksen tensors was obtained by Rivlin and Ericksen (Rivlin and Ericksen, 1955) as:

$$\mathbf{A}_{n+1}=\frac{\mathrm{d}}{\mathrm{d}t}\mathbf{A}_n+\mathbf{A}_n\mathbf{L}+\mathbf{L}^{\mathrm{T}}\mathbf{A}_n,\quad \mathbf{A}_0=\mathbf{I},\quad n=1,\ 2,\ \ldots \tag{3.15}$$

where **L** is the velocity gradient tensor and has the following definition:

$\mathbf{L}=\left(\frac{\partial\mathbf{u}}{\partial\mathbf{x}}\right)^{\mathrm{T}}=(\nabla\mathbf{u})^{\mathrm{T}}$, or $\mathrm{L}_{ij}=\frac{\partial u_i}{\partial x_j}$

It can be seen from equations (3.13) and (3.15) that the Jaumann stretching rate tensor and high-order Rivlin-Ericksen tensor are similarly constructed in form. Rivlin-Ericksen tensors can be obtained directly from the velocity field, without having to find the strain tensor. However, an alternative way of calculating Rivlin-Ericksen tensors was presented by Phan-Thien (2002), there we could also get a deeper understanding of the tensors: they are the high-order stretching rates of a fluid element. This is to say, they could be in accord with Jaumann stretching rate tensor in essence as we may expect.

Now let us turn back to the normal stress effect. This effect, which cannot be explained by the early models (Goodman and Cowin, 1971; Savage, 1979; Nunziato *et al*., 1980; Passman *et al*., 1980) as stated above, will be shown by model (3.12) in which the Jaumann stretching rate tensor is included. In order to see this, let us consider a simple shear flow where the velocity field takes the following form

$$u=\tfrac{1}{2}\dot{\gamma}y,\quad v=0,\quad w=0 \tag{3.16}$$

Then the velocity gradient tensor **L** can be given by

$$\mathbf{L}=\begin{bmatrix}0 & \frac{1}{2}\dot{\gamma} & 0\\ 0 & 0 & 0\\ 0 & 0 & 0\end{bmatrix} \tag{3.17}$$

In a simple shear flow, the first Rivlin-Ericksen tensor, *i.e.* twice strain rate tensor, can be calculated as

$$[\mathbf{A}_1] = \begin{bmatrix} 0 & \dot{\gamma} & 0 \\ \dot{\gamma} & 0 & 0 \\ 0 & 0 & 0 \end{bmatrix} \tag{3.18}$$

Then the second Rivlin-Ericksen tensor, *i.e.* the Jaumann stretching rate tensor, can be obtained from the first using (3.15) as

$$\begin{aligned} \mathbf{A}_2 &= \frac{\mathrm{d}}{\mathrm{d}t}\mathbf{A}_1 + \mathbf{A}_1\mathbf{L} + \mathbf{L}^{\mathrm{T}}\mathbf{A}_1 \\ &= \begin{bmatrix} 0 & 0 & 0 \\ 0 & 0 & 0 \\ 0 & 0 & 0 \end{bmatrix} + \begin{bmatrix} 0 & \dot{\gamma} & 0 \\ \dot{\gamma} & 0 & 0 \\ 0 & 0 & 0 \end{bmatrix}\begin{bmatrix} 0 & \dot{\gamma} & 0 \\ 0 & 0 & 0 \\ 0 & 0 & 0 \end{bmatrix} + \begin{bmatrix} 0 & 0 & 0 \\ \dot{\gamma} & 0 & 0 \\ 0 & 0 & 0 \end{bmatrix}\begin{bmatrix} 0 & \dot{\gamma} & 0 \\ \dot{\gamma} & 0 & 0 \\ 0 & 0 & 0 \end{bmatrix} \\ &= \begin{bmatrix} 0 & 0 & 0 \\ 0 & 2\dot{\gamma}^2 & 0 \\ 0 & 0 & 0 \end{bmatrix} \end{aligned} \tag{3.19}$$

It is clear from Expression (3.19) that model (3.12) which contains the Jaumann stretching rate tensor can give rise to normal stresses in a simple shear flow. Incidentally, in this flow all the other higher-order Rivlin-Ericksen tensors are zero and it can be verified for Cauchy-Green strain tensor that

$$\mathrm{C}_t(\tau) = \mathbf{I} + (\tau - t)\mathbf{A}_1 + \frac{1}{2}(\tau - t)^2\mathbf{A}_2 \tag{3.20}$$

It has been shown that the model of class (3.12) has a good ability in explaining the normal stress effect. However, the assumption of constant viscosity coefficient may be too sharp, because in general the viscosity may depend on shear rate. Thus the dynamical part of the constitutive equation can be expressed by the following function based on (3.12)

$$\overset{\circledcirc}{\mathbf{T}} = \check{\mathbf{H}}(\mathbf{D}, \mathring{\mathbf{D}}) \tag{3.21}$$

Note that the function $\check{\mathbf{H}}$ is assumed to be independent of stress, which seems to be confirmed by the work in literatures (Bagnold, 1954; Savage and Mckeown, 1983). In order to get a concrete dynamical model, some experimental results have to be referred to.

There is an extensive experimental data base in the literature on the flow properties of granular materials. One of the most influential pieces of work is due to Bagnold (1954), in which the experiments are carried out on suspensions of neutrally

buoyant particles in a Couette-flow apparatus. Based on the experimental results, Bagnold distinguished three flow regimes, namely a macro-viscous regime (low shear rate), a grain-inertia regime (high shear rate) and a transitional regime. The dependence of the shear and normal stress on the shear rate is found to be linear at low shear rate and quadratic at high shear rate. More recent experimental work includes that of Savage1983 and Hanes1985.

Based on the analysis of the above experimental results, a possible form for the viscosity coefficient was studied and the dynamical part of the hypoplastic constitutive model was presented by Wu (2006) as

$$\mathring{\mathbf{T}} = \eta_1 \sqrt{\eta_2^2 + \operatorname{tr} \mathbf{D}^2}\, \mathring{\mathbf{D}} \tag{3.22}$$

where parameters η_1 and η_2 in the model cannot be determined by conventional experiments, where the stresses are uniform and the strains homogeneous, but to be determined by fitting experimental data, as done by Hanes1985. Further analysis shows that equation (3.22) can describe fairly well the dependence of viscosity on shear rate in granular flow, namely linear dependence at low shear rate and quadratic dependence at high shear rate. This dynamical part will be introduced into the viscous hypoplastic constitutive model for frozen soil.

3.1.3 Static part of the viscous model

The statical part of the hypoplastic constitutive model for frozen soil will be formulated based on the rate-independent model proposed in Section 2, which is doubtlessly capable, on its own, to describe the main mechanical properties of frozen soil, as shown in Section 2.4. However, while it is combined with the above dynamical part to describe some rheological properties as well as rate-effect, an additional factor based on creep test should be introduced.

As we all know, creep is one of the most important rheological behaviors of frozen soil. However, the complexity of the microstructure change makes it very difficult to study the creep properties at microscope level. Based on the creep tests on frozen kaolin, Vyalov (1978) reported his first observation on the microstructure change of frozen kaolin during creep process, where *structure damage* and *particle*

orientation factors were introduced to characterize the microstructure changes. Another group of uniaxial creep tests on frozen Lanzhou loess was conducted by Zhang *et al*. (1995) at the temperatures of -5 and -10 °C, the water content of the specimens is 27-29 % and weight 1.89-1.98 g/m^3. The microstructure change of the specimen was analyzed with an electron microscope during the three stages of a typical creep test, which could be summarized as: 1) in the primary creep stage, the microstructure has the form of random permutation of soil grains without any structure damage, and the soil lumps are complete; 2) when the specimen enters the secondary creep stage, initial damage and radial micro-cracks occur gradually around the inherent defects and contact points between grains. Soil grains along the shear plane are reoriented and some soil lumps are crushed; and 3) in the tertiary creep stage, the reorientation of soil grains along the shear direction will become increasingly apparent, with the widening, extension then therefore cutting-through of micro-cracks. Zhang *et al*. (1995) also introduced factors similar to that of Vyalov (1978) to describe the evolution of microstructure damage during the creep process.

In view of the above instructive conclusions drawn from creep test, an additional factor, named creep damage factor f_{cd}, will be introduced into the rate-independent hypoplastic constitutive model proposed in Section 2. This factor can be formulated as

$$f_{cd} = 1 + \gamma \cdot \int_{t_1}^{t_2} \left\langle \dot{\mathrm{D}}(\tau) \right\rangle \mathrm{d}\tau \tag{3.23}$$

where γ is a parameter relating to the post failure behavior of frozen soil, when no failure occurs, γ can be any finite value, $\langle\ \rangle$ is Macaulay brackets and has the definition $\langle x \rangle := (x + |x|)/2$. $\dot{\mathrm{D}}(\tau)$ is the second-order time derivative of strain. The creep damage factor f_{cd} will enter the rate-independent model in the following form

$$\mathring{\hat{\mathbf{T}}} = c_1[\mathrm{tr}(\hat{\mathbf{T}}\text{-}\boldsymbol{s})]\mathbf{D} + c_2 \frac{\mathrm{tr}[(\hat{\mathbf{T}}\text{-}\boldsymbol{s})\mathbf{D}]}{\mathrm{tr}(\hat{\mathbf{T}}\text{-}\boldsymbol{s})}(\hat{\mathbf{T}}\text{-}\boldsymbol{s}) + f_{\varepsilon} \cdot f_{cd} \cdot \left[c_3(\hat{\mathbf{T}}\text{-}\boldsymbol{s})^2 + c_4(\hat{\mathbf{T}}\text{-}\boldsymbol{s})_{\mathrm{d}}{}^2 \right] \frac{\|\mathbf{D}\|}{\mathrm{tr}(\hat{\mathbf{T}}\text{-}\boldsymbol{s})} \tag{3.24}$$

3.1.4 The complete visco-hypoplastic constitutive model

When combining the statical part (3.24) and the dynamical part (3.22), the

complete constitutive equation for both statical and dynamical behavior of frozen soil can be obtained as:

$$\dot{\mathbf{T}} = c_1[\mathrm{tr}(\mathbf{T}\text{-}\boldsymbol{s})]\mathbf{D} + c_2 \frac{\mathrm{tr}[(\mathbf{T}\text{-}\boldsymbol{s})\mathbf{D}]}{\mathrm{tr}(\mathbf{T}\text{-}\boldsymbol{s})}(\mathbf{T}\text{-}\boldsymbol{s}) + f_\varepsilon \cdot f_{cd} \cdot \left[c_3(\mathbf{T}\text{-}\boldsymbol{s})^2 + c_4(\mathbf{T}\text{-}\boldsymbol{s})_d^{\,2} \right] \frac{\|\mathbf{D}\|}{\mathrm{tr}(\mathbf{T}\text{-}\boldsymbol{s})} + \eta_1 \sqrt{\eta_2^2 + \mathrm{tr}(\mathbf{D}^2)}\dot{\mathbf{D}} \quad (3.25)$$

The above constitutive equation can be applied to the entire process from solid-like to fluid-like behavior. Unlike most of the conventional models, where constitutive equations for the statical and dynamical regimes are formulated and applied separately, the above constitutive equation makes no distinction between them.

To this stage, the visco-hypoplastic constitutive model for frozen soil has been set up, the consequent question is how does this viscous model perform. This will be checked in the next section.

3.2 Verification of the visco-hypoplastic constitutive model

As stated at the beginning of this section, the visco-hypoplastic constitutive model is expected to be able to describe some rheological behaviors and the effect of loading rate on the mechanical behaviors of frozen soil. In order to check this, both creep tests at different stress levels and compression tests at different strain rates on frozen soils are simulated with the proposed viscous model in this section.

3.2.1 Simulation of compression tests at different strain rates

As previously mentioned, the stability of structures in cold regions can be affected to a large extent by the construction speed (loading or unloading rate). In order to get a better understanding of the rate-effect on the mechanical behaviors of frozen soil, some uniaxial compression tests at different strain rates were conducted on frozen Fairbanks silt by Zhu and Carbee (1984). The soil tested has a plastic limit of 34.2% and liquid limit of 38.4%. Specimens were prepared by compressing the soil to the desired density in acrylic plastic molds and had the dimensions of 70 mm in diameter and 152 mm in length. After the specimens were saturated with a vacuum pump, they were placed into a freezing cabinet and frozen quickly to avoid ice lens

during freezing. 6 different loading rates (50, 5, 1, 0.1, 0.01 and 0.001 cm/min, corresponding to the strain rates of 5.5×10^{-2}, 5.5×10^{-3}, 1.1×10^{-3}, 1.1×10^{-4}, 1.1×10^{-5}, 1.1×10^{-6} s^{-1}) and 7 different temperatures (-0.5, -1.0, -2.0, -3.0, -5.0, -7.0 and -10.0 $^{\circ}$C) were employed in these tests. The procedures of the test can be summarized as: firstly, the prepared specimens were kept at the same temperature as that planned for the test for 12 hours in a constant temperature cabinet; then the sample was placed on a screw-driven universal material testing machine to perform the uniaxial compressive test at a constant deformation rate and a constant temperature. A data acquisition system automatically recorded the axial load and deformation during the entire process of the compression test. Then the axial stress and strain were calculated, and the corresponding stress-strain curves were plotted.

Compression tests at 4 different strain rates at the temperature of -3 $^{\circ}$C are simulated by the proposed visco-hypoplastic constitutive model. The simulation is carried out according to the following procedures: 1) an acceleration phase is inevitable for an initially stationary specimen to deform afterwards at a constant strain rate, the acceleration is assumed to be constant in this phase; 2) when the target strain rate is reached, the specimen will be compressed at a constant strain rate till failure occurs, the creep acceleration in this phase is 0. Consequently, the model will return to the rate-independent one as talked in Section 2. In both phases, the creep damage factor f_{cd} can be obtained as 1, thus parameter γ can be any finite value. The other parameters in the visco-hypoplastic model and the strain acceleration in the first phase are chosen as follows (also in Table 3.1): c_1 = -98.31, c_2 = -905.48, c_3 = -858.98, c_4 = 1146.98, s = 207.1 kPa, β = 0.005, $\eta_2 = 10^{-6}$ s^{-1}.

Table 3.1 Parameter in the visco-hypoplastic constitutive model

$D_1(s^{-1})$	1.1e-6	1.1e-5	1.1e-4	1.1e-3
α	-0.004	-0.0006	-0.00001	-0.002
η_1 ($kP_a \cdot s^2$)	4.6e15	1.3e14	1.95e12	1.65e10
$\dot{D}_1$ (s^{-2})	-1.0e-10	-1.0e-8	-1.4e-6	-1.53e-4

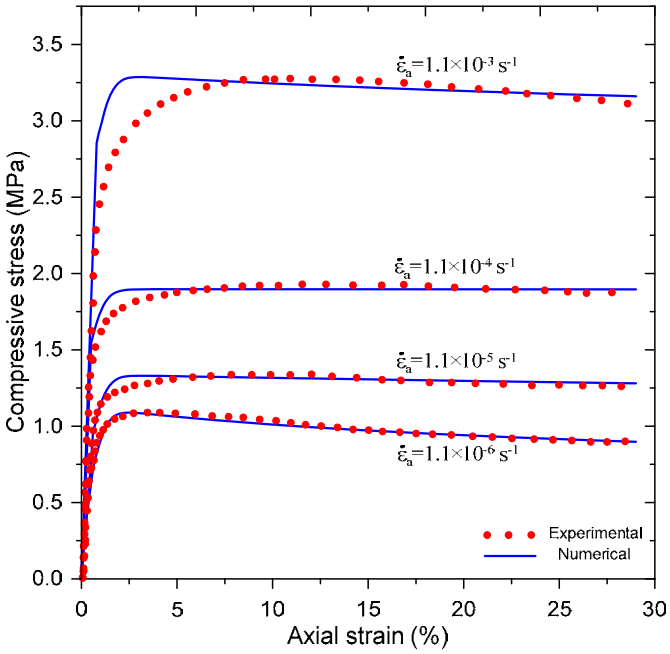

Fig. 3.1 Stress-strain relationship at different strain rates (-3 °C)

By using the above parameters, the simulated stress-strain relationship of frozen Fairbanks silt in uniaxial compression tests at different strain rates is presented in Figure 3.1 together with the experimental results. From the experimental results we can see that: 1) the strength develops with the deformation of specimen then followed by strain softening during each compression test; 2) the responses of the specimen to different strain rates are different, the higher the rate is, the tougher the specimen will be. Therefore an increase in the strength (as well as the initial tangent modulus) of the specimen can be observed with the increase of strain rate; and 3) the strain at failure also has a tendency to increase with the strain rate. Comparison between the experimental and numerical results shows that all the above changing rules can be described quite well by the proposed visco-hypoplastic constitutive model.

In the work by Zhu and Carbee (1984), the peak compressive strength and initial tangent modulus were also analyzed: a logarithmic function and a power function were proposed to describe the effect of strain rate on the peak strength and initial modulus, respectively. Here these two quantities at different strain rates are also obtained with the viscous model, the results are shown in Figures 3.2 and 3.3. It can be seen from Figure 3.2 that the peak strength increases approximately linearly with the strain rate in a semi-logarithmic coordinate system, which means that a

logarithmic relationship can be drawn between the peak strength and strain rate. Recalling the relationship obtained by Zhu and Carbee (1984), we can soon note that the two relationships are similar to each other. In Figure 3.3 the change of initial tangent modulus with strain rate is presented, like the above logarithmic relationship obtained in Figure 3.2, a similar logarithmic relationship between the initial modulus and strain rate can also be obtained from Figure 3.3. According to the conclusion by Zhu and Carbee (1984), a numerical fitting based on a power function is also presented in Figure 3.3. By comparing the two curves in Figure 3.3 we can find that it seems better to use the logarithmic function to describe the strain rate effect, as done by Parameswaran (1980), Wu *et al*. (1993) and Li *et al*. (1995).

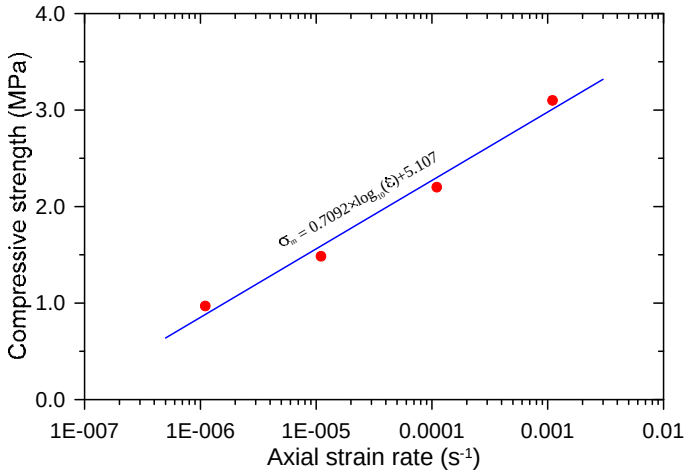

Fig. 3.2 Change of compressive strength with strain rate

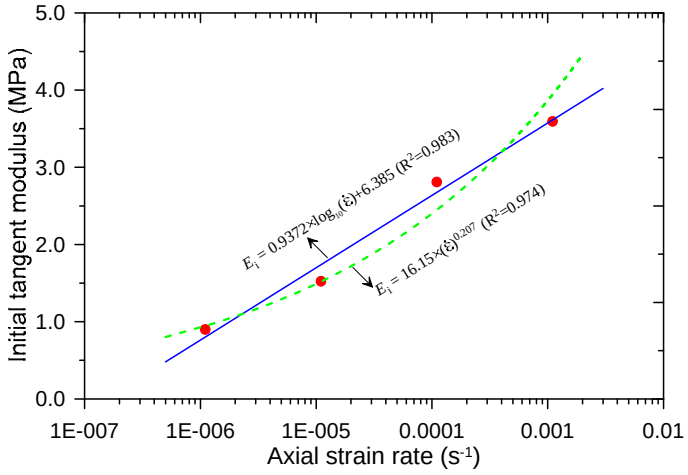

Fig. 3.3 Change of initial tangent modulus with strain rate

3.2.2 Simulation of creep tests at different stress levels

The creep properties of frozen soil, like creep strength and creep deformation characteristics, are important information required in the design of structures in permafrost regions, since the long term stability of the structures is heavily dependent upon the creep properties of frozen soil. As we may expect, the proposed visco-hypoplastic constitutive model should be able to describe the creep properties of frozen soils. This will be ascertained by simulating some uniaxial creep tests conducted by Orth (1986) at different temperatures and stress levels.

Karlsruhe Medium sand is chosen as the study material in Orth's work, the particle gravity of this sand is 26.5 kN/m^3. In the creep tests, the dry specimens are also prepared with the sand pluviation method, as talked in Subsection 2.4.1. The prepared specimen has a dry bulk density of 17.2 kN/m^3 and water content of 18%. The dimensions of the specimen are 10 cm in diameter and also 10 cm in height. All the creep tests are carried out in a cold room, which could insure a more uniform temperature field in the specimen than a locally cooled device can do. In the tests, different temperatures (-2, -5, -10, -15 and -20 $^\circ$C) are concerned, depending on which, different stress levels, from lowest 1.0 MPa to highest 14.0 MPa, are also considered. During the uniaxial creep tests, axial strain, axial force (stress) and axial strain rate are measured. For more detailed information about the test, the original publication (Orth, 1986) can be referred to.

Since all the creep tests are conducted at a constant temperature and constant stress level, constant temperature can be easily obtained by controlling the room temperature, constant stress level can also be maintained without any difficulty. Here the importance should be attached to the process before the target creep stress is reached, which can be compared to the process before the target strain rate is reached in the compression test at constant strain rate in Subsection 3.2.1, therefore, in order to simulate the creep tests, the procedures can be laid out as: 1) a uniform acceleration phase in the specimen is also necessary for conducting the creep test, like the acceleration phase before compressing the specimen in the above subsection.

However, the governing condition for stopping acceleration here is not as clear as that in the compression test, where strain rate can be taken as the governing condition, here may only by assumption. At the end of this short acceleration phase, the sum of the statical and dynamical stress is normally less than the target creep stress, which requires 2) a compression phase of constant strain rate. In this phase, the dynamical stress will keep constant as a result of the vanishing creep acceleration, the statical stress will increase till the sum of the two stresses reaches the target creep stress. The model in this phase will recover to the rate-independent type which has already been dealt with in Section 2; and 3) when the target creep stress is reached, it will be kept constant. Meanwhile, the creep test is initiated.

Table 3.2 Governing equation corresponding to the 3 phases

Phase	Equation	Equation type	Boundary condition (Known)	Unknown	Solving method in MATLAB
1	$\dot{T}_2 = 0$	ordinary differential equation	D_1, $\dot{D}_1$, initial D_2	D_2; $\dot{\hat{T}}_1$, $\dot{\hat{T}}_2$	ode45
2	$\dot{\hat{T}}_2 = 0$	linear equation	D_1	D_2; $\dot{\hat{T}}_1$	solve
3	$\dot{T}_1 = 0$ $\dot{T}_2 = 0$	ordinary differential equation system	initial D_1 initial D_2	D_1, D_2; $\dot{D}_1$ $\dot{\hat{T}}_1$, $\dot{\hat{T}}_2$	ode45

Corresponding to the above three phases, the governing equation or equation system needed to be solved in each phase is listed in Table 3.2. Among the three-phase simulations, the most interesting and noteworthy simulation is in phase 3), which can be briefly described as: firstly, at the beginning of the first time step, the axial strain rate and radial strain rate should be assigned with two initial values, then the constitutive model expressed by two ordinary differential equations can be solved, the solution will be new values for the axial strain rate and radial strain rate at the end of the first time step; secondly, based on the above solution, the creep acceleration,

statical stress (rate) and dynamical stress (rate) can be obtained, which are required in the calculation of the second time step; finally, the new values for the axial strain rate and radial strain rate will serve as the initial values for the calculation of the second time step, before which the stress state should be updated. With such iterative algorithm, the whole creep process can be simulated.

In this section, only the creep tests at the temperature of -10 $^{\circ}$C are simulated. The parameters for simulating the creep tests at different stress levels are obtained as follows: c_1 = -83.57, c_2 = -769.66, c_3 = -730.13, c_4 = 974.93, s = 3061.9 kPa, β = 0.005, $\eta_2 = 10^{-6}$ s^{-1}, the other parameters in the model and some initial conditions for each phase are presented in Table 3.3 (for the model recovers to the rate-independent one in the second phase, the strain rate in this phase can be any finite value, thus omitted in the table).

Table 3.3 Model parameters and initial conditions

	10000	9000	8000	7000	6000	3000
α	-0.18	-0.006	-0.003	-0.0003	-0.0003	-0.0003
γ	64200	97200	24200	180200	0.001-0.1	——
η_1 ($kP_a \cdot s^2$)	1.95e12	1.6e12	1.2e12	0.8e12	0.2e12	1.2e11
STAGE I						
D_1 (s^{-1})	-5e-5	-4.24e-5	-3.73e-5	-0.42e-5	-0.1e-5	-0.25e-6
$\dot{D}_1$ (s^{-2})	-2e-7	-1.5e-7	-1.312e-7	-0.8e-7	-0.6e-6	-0.15e-6
STAGE III						
D_1 (s^{-1})	-4.3e-5	-3.1e-5	-3e-5	-2.2e-5	-1.2e-5	-1e-5
D_3 (s^{-1})	2.2e-5	1.5e-5	1.5e-5	1.1e-5	6e-6	5e-6

The simulated axial strain and its rate of the creep tests are presented in Figures 3.4 and 3.5, respectively. At this stage, it should be noted that, for frozen soils, failure in a creep test is often defined as a point with the minimum creep rate in the creep

rate-time curve, meanwhile from which the creep rate starts to accelerate. To describe this point, two important concepts in creep, namely the minimum creep rate and the time to this minimum rate, are often resorted to. These two concepts are also often introduced to develop creep models (*e.g.* Assur, 1980; Fish, 1982) and interpret the predictive ability of the models. From Figures 3.4 and 3.5 we can see that the specimen experiences a change from a state without failure (for stress level at 3000 kPa) to a failure state (for all stress levels except 3000 kPa) as the creep stress level increases, and the time to failure decreases with the increase of creep stress (note the abscissas in Figures 3.4 and 3.5), these properties can be well captured by the proposed viscous model. Figures 3.4 and 3.5 also show the three typical stages of the creep of frozen Karlsruhe Medium sand. The complete process of the change of strain rate can be described as: the strain rate continuously decreases from the outset of the creep test until it reaches a minimum, then continuously increases till creep rupture. This implies that the secondary creep is, actually, an inflection point in the strain-time plot. However, it is often regarded as a “steady-state” creep stage, since the creep rate around the minimum rate, or specifically, over a certain time range after the minimum rate changes very little in a linear Cartesian coordinate system. It can be seen from the comparison results that the evolution of strain and of strain rate through the three creep stages can be well reproduced by the visco-hypoplastic model, except for low stress level at which small discrepancy occurs. This maybe could attribute to the low initial rate at the beginning of the creep test, certain rate level should be maintained to keep the creep stress constant in the specimen.

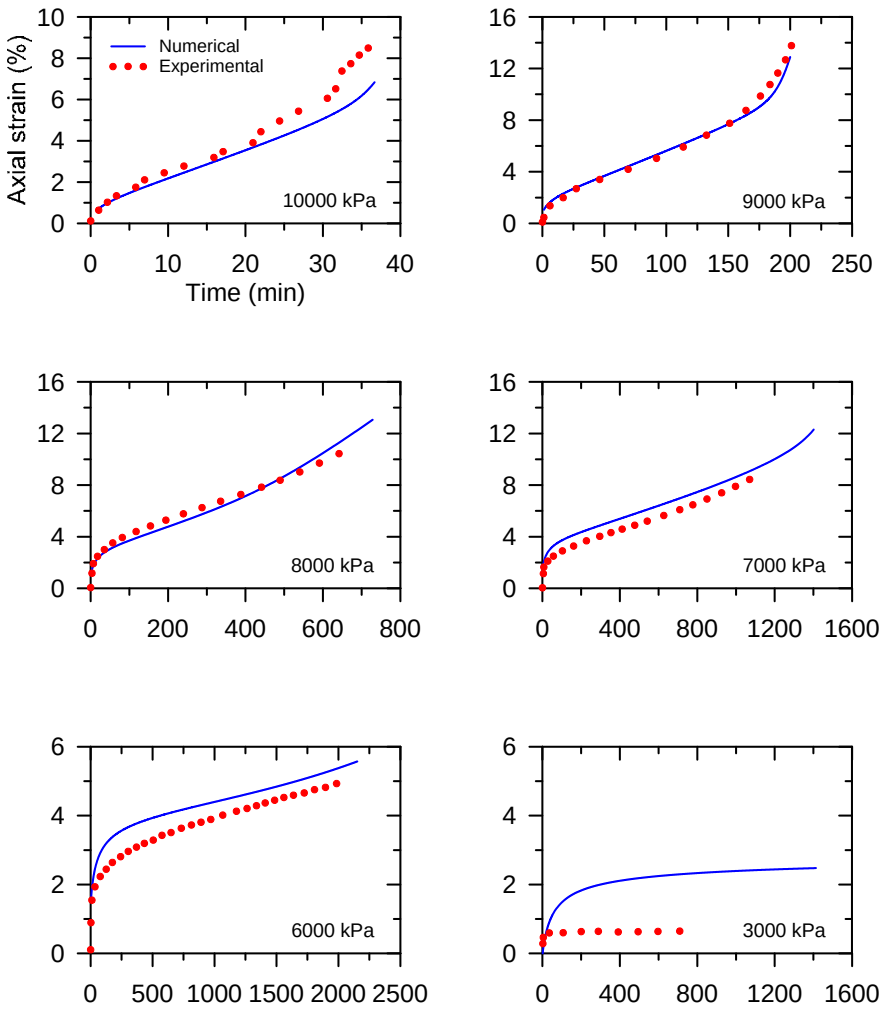

Fig. 3.4 Change of creep strain with time at different stress levels

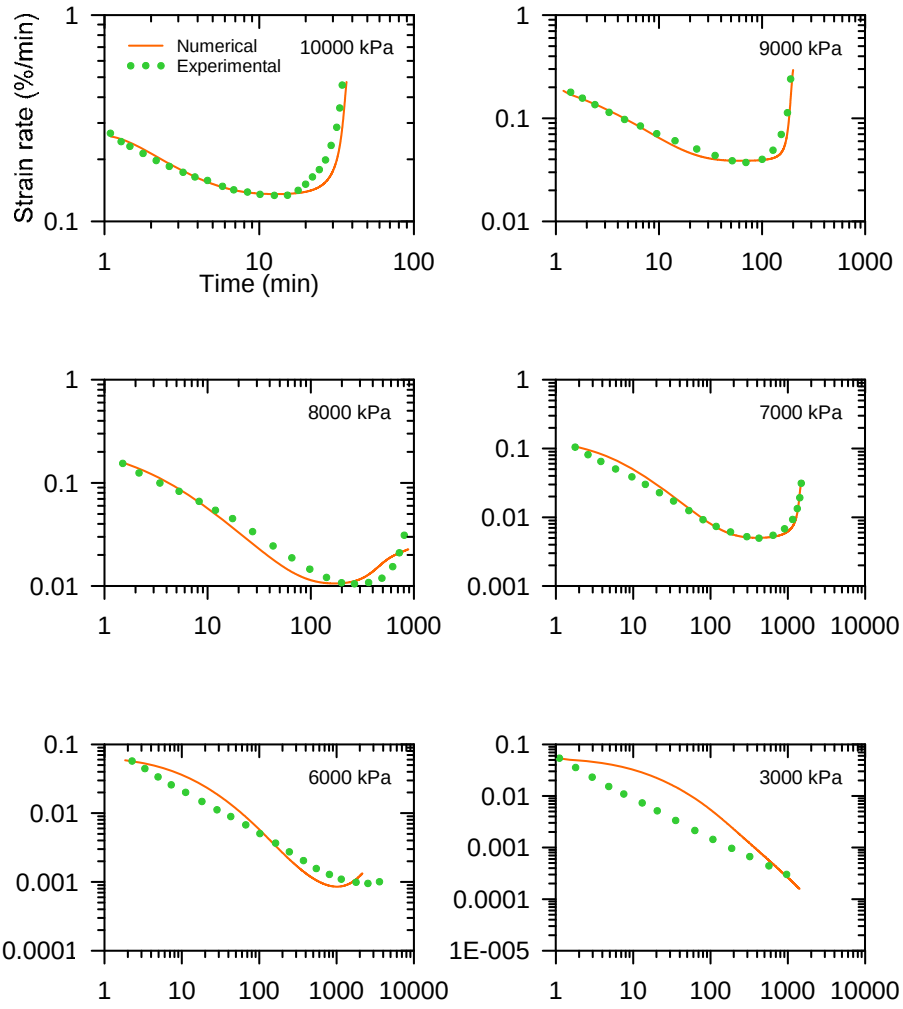

Fig. 3.5 Change of creep strain rate with time at different stress levels

Since the proposed visco-hypoplastic constitutive model is formulated in rate type, *i.e.* the total stress rate is composed of the statical stress rate and dynamical stress rate, here the changes of the statical stress, dynamical stress and their rates are also analyzed during the whole process of the creep test.

The evolutions of the statical stress and dynamical stress with time at different stress levels are shown in Figure 3.6. It can be seen from Figure 3.6 that three stages, corresponding to the primary, secondary and tertiary creep stage, are also recognizable. In the first stage, the statical stress (solid line) continuously increases from the beginning of the creep test; then it will reach a maximum corresponding to the infection point in the creep curve, which represents the second stage; subsequently, in the third stage the statical stress will decrease till the end of the test then creep

rupture comes. As the statical stress changes very little, even unperceivable, at relatively low creep stress in the full figure for the complete creep process, the detailed change of statical stress is presented in Figure 3.7. From Figure 3.7 we can easily realize that the above variation pattern for the statical stress drawn from Figure 3.6 is further confirmed. However, it should be noted that this conclusion is obtained for the case where creep failure occurs. When the specimen does not fail at lower creep stress level, *e.g.* 3000 kPa, only the first stage can be observed, in which the statical stress continuously increases to a constant value, as shown in Figure 3.7. Besides, it can also be seen from Figures 3.6 and 3.7 that the dynamical stress (dash line) changes in a manner axially symmetric to that of statical stress, no matter the specimen fails or not. Obviously, this will generate a constant total stress, which is precisely required by a creep test.

The changes of the statical and dynamical stress rate at different creep stresses are also presented. From Figure 3.8 we can see that, throughout the three typical creep stages, the statical stress rate (solid line) decreases all the time. Likewise, three stages for the variation of statical stress rate can also be obtained, namely decrease from a positive finite value to 0 in the first stage, an approximate 0 in the second stage and decrease from 0 to a negative value in the third stage. Owing to the poor perceivability in the full figure, detailed change of the stress rates (both statical and dynamical) at relatively low stress levels is presented in Figure 3.9, from which we can see different patterns of the change of stress rates: if the specimen fails in creep test, the statical stress rate will continuously decrease from a positive to a negative, otherwise, it will only decrease from a positive to 0 and then stay there. Figures 3.8 and 3.9 also show that the change manner of the dynamical stress rate is right opposite to that of the statical stress rate. This will lead the total stress rate to be 0, *i.e.* the total stress being constant. Again, the creep condition is fulfilled.

Recalling the definition of creep failure, we know that failure will take place when the minimum creep rate occurs, or equivalently, when the creep acceleration becomes 0 (opposite signs are necessary on the two sides of 0), the specimen will fail. Therefore, the creep acceleration of a value of 0 can be taken as the symbol of failure.

In this study, the evolutions of the creep acceleration at different stress levels are shown in Figures 3.10 and 3.11. It can be seen that the creep acceleration is negative at the beginning of the creep test for all stress levels. With the proceeding of the test, the creep acceleration will continuously increase no matter it surpasses 0 or not. It is obvious that for the case when the creep acceleration does not surpass 0, *e.g.* at the stress level of 3000 kPa, the specimen will not fail, no matter how long the test lasts. Otherwise, creep failure will occur in the specimen, as at relatively high stress levels. The failure points are also marked on the acceleration-time curves, it can be seen that the time to failure will decrease with the creep stress level, as shown by points A and B in Figure 3.11. It can be easily noted that this is consistent with the above conclusion.

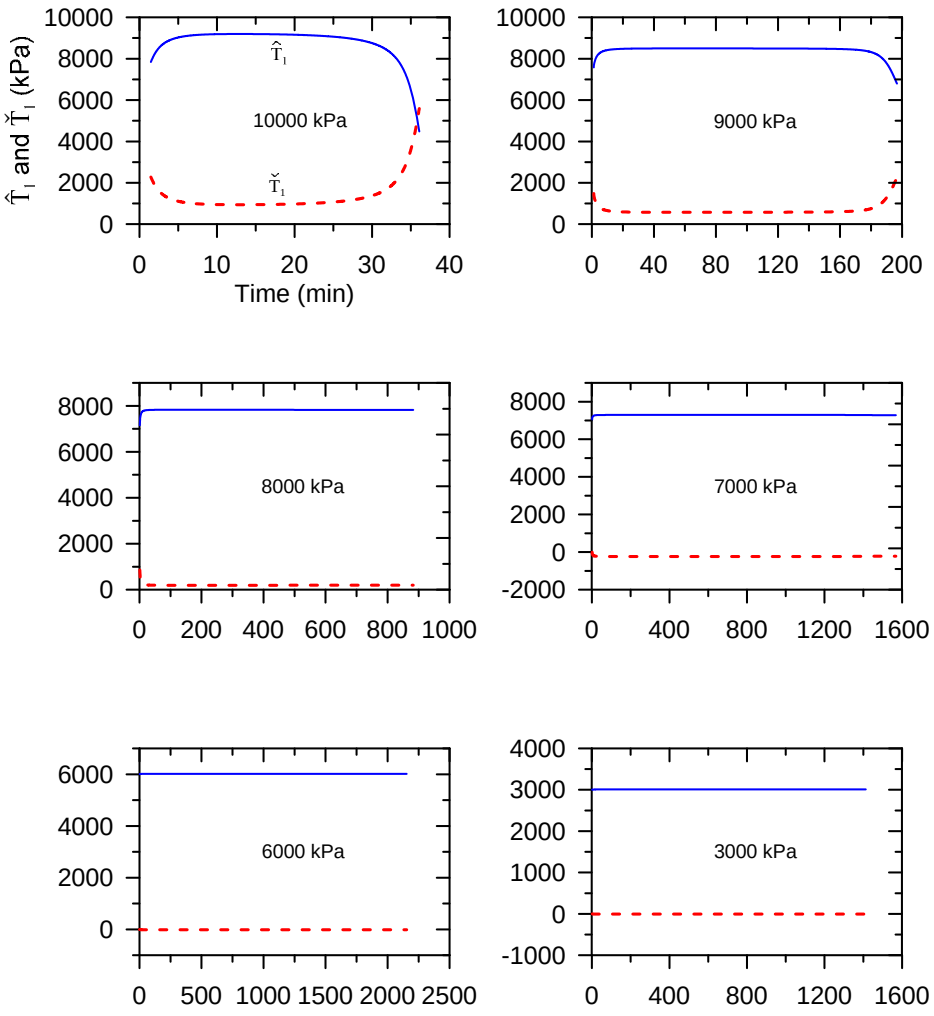

Fig. 3.6 Changes of static and dynamic stress with time at different stress levels

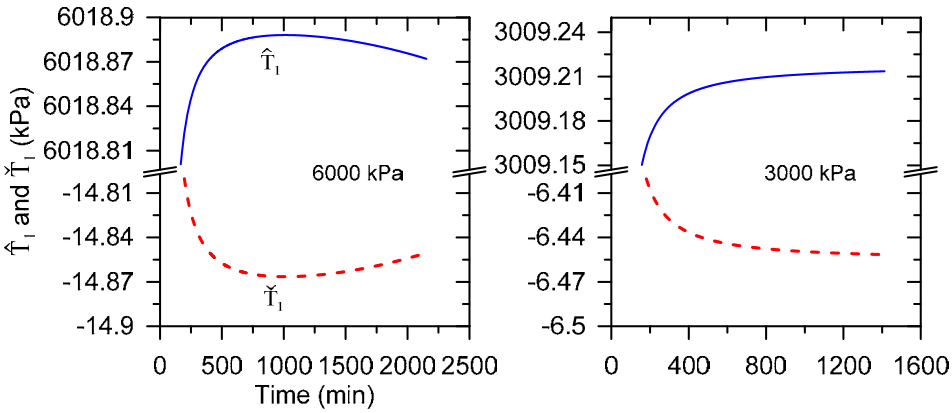

Fig. 3.7 Detailed changes of static and dynamic stress at 6000 and 3000 kPa

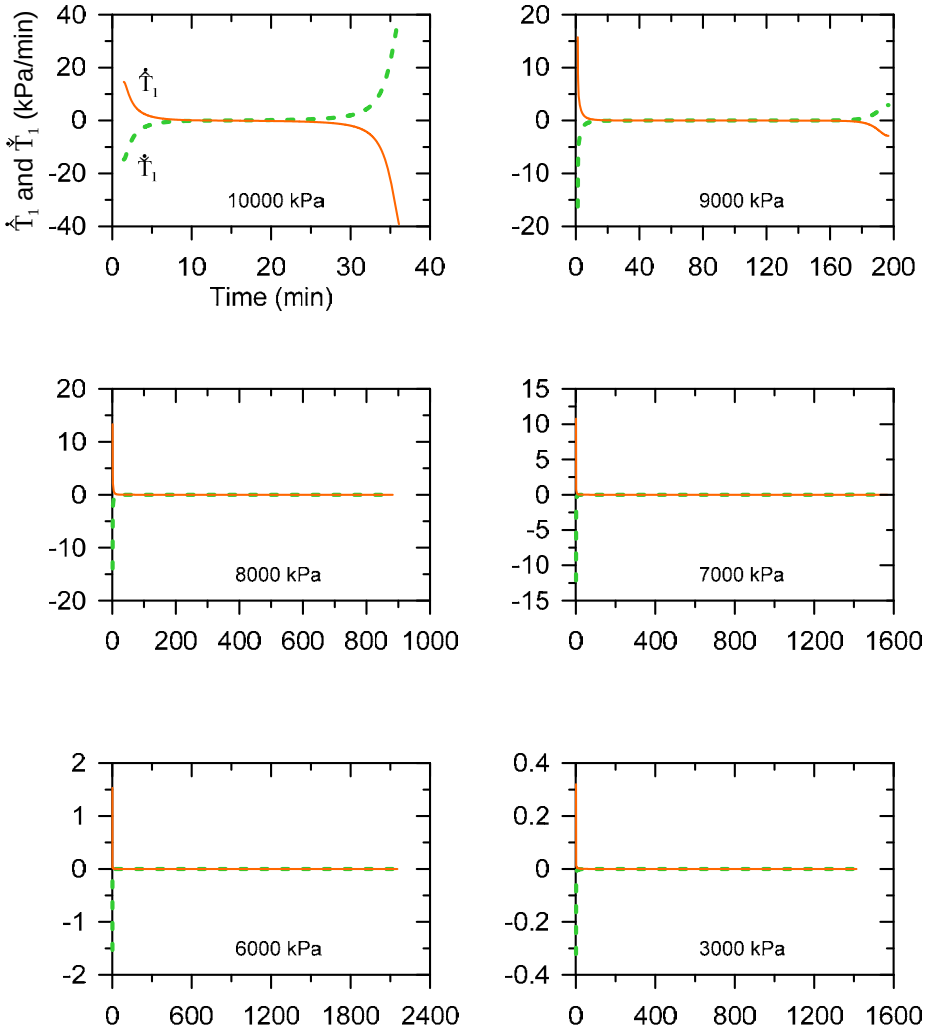

Fig. 3.8 Changes of static and dynamic stress rate with time at different stress levels

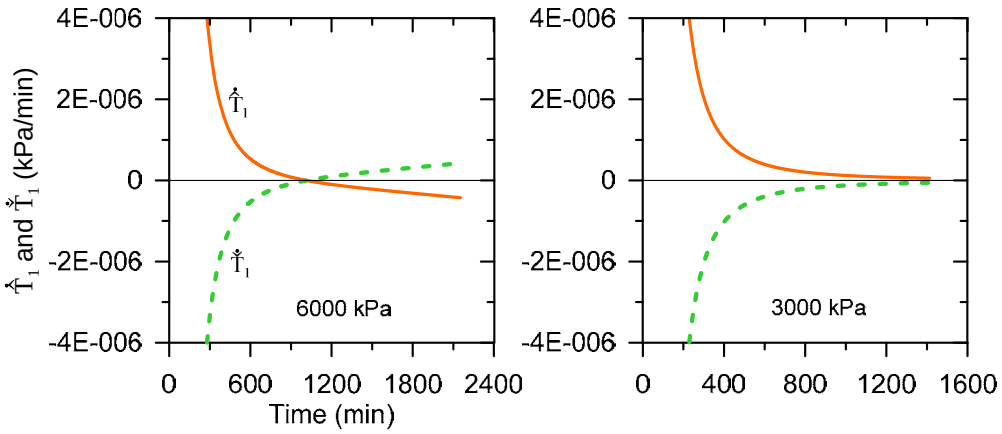

Fig. 3.9 Detail changes of static and dynamic stress rate with time around failure

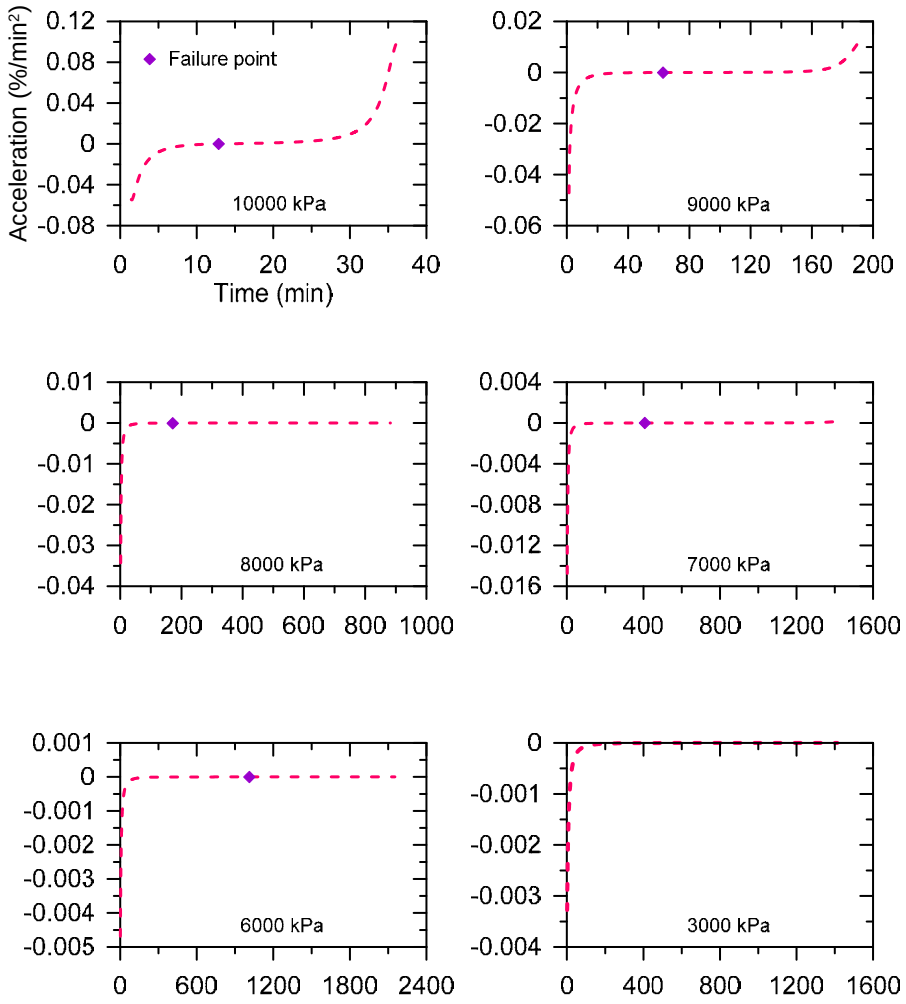

Fig. 3.10 Change of creep acceleration with time at different stress levels

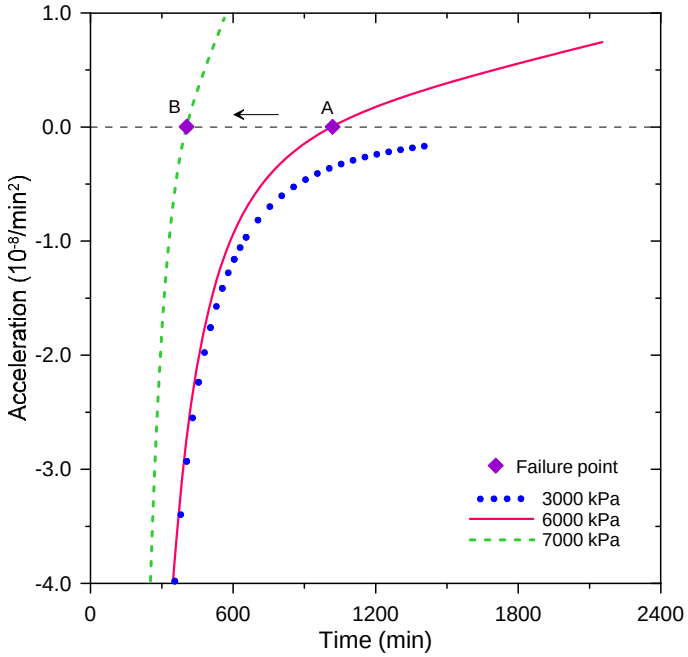

Fig. 3.11 Detail change of creep acceleration around failure

3.3 Discussion on the visco-hypoplastic constitutive model

A visco-hypoplastic constitutive model is proposed for frozen soil in this section. It is interesting that both compression test at different loading rates and creep test can be simulated by the model, this is quite infrequent in material modeling. By simulating some uniaxial compression tests at different loading rates and creep tests at different stress levels, the performance of the model is demonstrated. From the simulation results it is easy to find that the proposed model can describe fairly well the viscous behaviors of frozen soils, such as rate-dependence of compression strength and strain (rate) evolution in a creep test.

Besides, it is noteworthy that the proposed model can describe the three-stage creep process in a unified way, therefore it does not have the limitations of the special models which are only valid for one or two of the three stages, *e.g.* the primary creep model only works well for the primary stage of the creep test, and normally underestimates the strain and strain rate when the test enters the secondary and tertiary stage; the secondary creep model generally overestimates the strain and

underestimates the strain rate for the primary creep stage, and slightly underestimates both the strain and its rate for the tertiary stage. From this point of view, the proposed visco-hypoplastic model is superior to either, not only a fairly accurate fit can be made for both strain and strain rate, it can also elaborate the evolution of creep acceleration through the test.

4 A hypoplastic creep model for frozen soil

As always emphasized in Section 3, the viscous behavior of frozen soil, especially creep, is crucial in various engineering activities in permafrost regions, therefore it will be never excessive to put effort into the study of the creep of frozen soils. In this section, without repeating the importance of creep to the stability of structures on frozen ground, another hypoplastic model is developed. The model is formulated by introducing a function of deformation into the non-linear terms of the original hypoplastic constitutive model proposed by Wu (1992), meanwhile, the Euclidean norm of the strain rate in the original model is removed in order to break the strong restriction of rate-independence. Like the viscous model in Section 3, the model can also describe the three-stage creep process in a unified way. Parameters in the model can be obtained from the creep rate curves, and no distinction has to be made between the cases with and without failure. The proposed model is then validated by simulating some creep tests at different temperatures and stress levels.

4.1 Hypoplastic creep model

Recalling the original hypoplastic constitutive model proposed by Wu (1992), we know that the model is rate-independent, thus cannot describe the creep behavior of materials. The reason for this lies in the strong restriction: the stress rate is positively homogeneous of the first order in strain rate (see Equation (2.3)). In order to enable the model to describe creep behaviors, this restriction should be broken. This can be accomplished by removing the Euclidean norm of the strain rate in the non-linear terms of the model. Besides, the original model is formulated, based on the second restriction, by stress rate being a homogeneous tensor function of stress (see Equation (2.4)). Keeping this in mind and noting simultaneously that the creep stress in a creep test should be kept constant, *i.e.* the stress rate during the creep test should be maintained at 0, a stress-independent creep strain rate will be obtained from the

original model. Obviously, this is in conflict with the creep results obtained at different stress levels. Therefore, in order to get an appropriate creep model, the second restriction should also be relieved.

Following the way of dealing with the cohesion of frozen soil in Sections 2 and 3, let us consider the following hypoplastic model

$$\dot{\mathbf{T}} = c_1[\mathrm{tr}(\mathbf{T}\text{-}\boldsymbol{s})]\mathbf{D} + c_2\frac{\mathrm{tr}[(\mathbf{T}\text{-}\boldsymbol{s})\mathbf{D}]}{\mathrm{tr}(\mathbf{T}\text{-}\boldsymbol{s})}(\mathbf{T}\text{-}\boldsymbol{s}) + f(\mathrm{D})\cdot\left[c_3(\mathbf{T}\text{-}\boldsymbol{s})^2 + c_4(\mathbf{T}\text{-}\boldsymbol{s})_{\mathrm{d}}^2\right] \tag{4.1}$$

in which $f(\mathrm{D})$ is a scalar function regarding deformation. When multiplying all the stress terms or strain rate terms on the right side of (4.1) by any positive scalar, we can find that the scalar cannot be picked out as a common factor. Therefore, the two restrictions mentioned above are relieved, *i.e.* model (4.1) is not homogeneous in stress or strain rate. The inhomogeneity of model (4.1) renders itself a possibility to describe the creep behaviors of frozen soil.

To this stage, the immediate task is to determine a concrete form for the deformation function. For this purpose, let us turn back to the experimental results of uniaxial compression creep tests at different stress levels and temperatures (Orth, 1986), in which the evolution of creep strain rate can be summarized as: for a complete three-stage creep process, the strain rate continuously decreases in the primary stage, subsequently takes its minimum and then increases continuously in the tertiary stage till creep rupture. This kind of evolution can be well described by

$$\log[f(\mathrm{D})] = a[\log(l) + d] + \frac{b}{\log(l) + d} + c \tag{4.2}$$

where a, b, c and d are parameters depending only on stress at a certain temperature, l is the accumulation of deformation as talked in Section 2. Further study of the deformation function shows that, the first term on the right side of Equation (4.2) dominates in the primary creep stage and the second term is dominant in the tertiary creep stage. Similarly constructed constitutive equation can also be found in the work by Okubo *et al*. (1991) for various rocks.

4.2 Validation of the hypoplastic creep model

In this section, we proceed to validate the hypoplastic creep model proposed in Section 4.1 by simulating some creep tests (Orth, 1986) at different temperatures and stress levels. Before the simulation, the parameters in the hypoplastic creep model should be determined according to the creep rate curves.

4.2.1 Determination of the parameters in the creep model

There are in total 8 parameters in the hypoplastic creep model, namely, 4 material parameters c_i (i = 1, 2, 3, 4) from the original model (Wu, 1992), 4 other parameters, a, b, c and d, in the introduced function of deformation. As the Euclidean norm of strain rate in the non-linear terms of the original model is removed, it is recommended that c_3 and c_4 in the hypoplastic creep model should be obtained by multiplying the original ones by a factor equivalent to the norm, while keep c_1 and c_2 unchanged.

As stated in Section 4.1, the creep rate can be described by Equation (4.2), and the first and the second term on the right side of (4.2) dominate in the primary and the tertiary creep stage, respectively. Consequently, in the primary creep stage, the creep rate can be approximated by

$$\log[\, f(\mathrm{D})] = a[\log(l) + d\,] \tag{4.3}$$

It can be easily found from (4.3) that parameter a can be determined from the slope of the creep rate-deformation curve in log-log plot. d is a global translation parameter and has no effect on parameter a, thus should be determined in the end. In the tertiary creep stage, the creep rate can be approximated by

$$\log[\, f(\mathrm{D})] = \frac{b}{\log(l) + d} \tag{4.4}$$

Based on an optimal fit to the experimental results of creep tests, parameter b in (4.4) then can be obtained from the intercept at a relatively large time point in the creep rate - deformation curve in a twice logarithmic coordinate system.

Once parameters *a* and *b* are determined, parameters *c* and *d* can also be obtained by substituting the minimum creep rate and its derivative into (4.2), then solving the equation system with respect to variables *c* and *d*.

4.2.2 Simulation of compression creep tests

Two groups of uniaxial compression creep tests at the temperatures of -2 and -10 °C are simulated in this section. The tests were conducted by Orth (1986) on frozen Karlsruhe medium sand at different creep stresses. For the tests at -2 °C, creep stresses from 1000 to 4000 kPa were adopted, while for -10 °C, stresses from 1000 to 10 000 kPa were used. Taking the tests at the temperature of -10 °C as an example, the 4 material parameters in the hypoplastic creep model can be obtained as: c_1 = -68.82, c_2 = -673.56, c_3 = 0.0768 $kPa^{-1}\cdot s^{-1}$, c_4 = -0.0256 $kPa^{-1}\cdot s^{-1}$, and the cohesion of the frozen sand *s* = 3061.9 kPa. For the creep stress at 10 000 kPa, the other 4 parameters can be obtained according to the calibration process in Subsection 4.2.1 as: *a* = -0.3753, *b* = -0.1086, *c* = -8.1151, *d* = -3.435. When more sets of parameters at other creep stresses are determined, see Figure 4.1, it can be easily found that 4 linear relationships can be drawn separately between each parameter and creep stress level. The 4 relationships are presented in below, in which the creep stress has the dimension of [MPa]. It will be interesting to note that, even in the case that no creep failure occurs in the specimen, such as 1000 and 3000 kPa at -10 °C, the parameters can still be covered by the linear relationships.

$$a = 0.066 \times T - 1.076$$

$$b = 0.034 \times T - 0.462$$

$$c = 0.652 \times T - 14.52$$

$$d = 0.522 \times T - 8.883$$

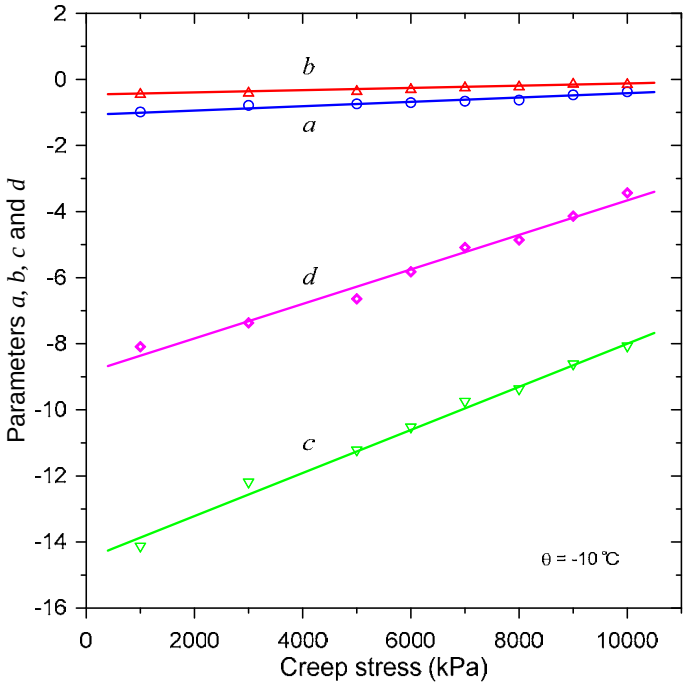

Fig. 4.1 Relationships between the parameters and creep stress

Since the parameters in the hypoplastic creep model have been determined, let us turn back to the simulation of the creep tests. As is known to all, in a uniaxial compression creep test, no radial stress should be applied, meanwhile the axial stress should be kept constant, *i.e.* the axial stress rate will be 0. These points will serve as the boundary conditions when solving the governing equations of a uniaxial creep test. Keeping these points in mind, the axial strain rate in a uniaxial compression creep test can be calculated according to (4.1) as:

$$\mathrm{D}_1 = -\frac{c_3 + \frac{4}{9}c_4}{c_1 + c_2}(\mathrm{T}_1 - \mathrm{s}_1)\cdot f(\mathrm{D}) \tag{4.5}$$

Substituting (4.2) into (4.5) then taking the logarithm of both sides of the equation, we can get

$$\log(\mathrm{D}_1) = a[\log(l) + d] + \frac{b}{\log(l) + d} + c + \log[-\frac{c_3 + \frac{4}{9}c_4}{c_1 + c_2}(\mathrm{T}_1 - \mathrm{s}_1)] \tag{4.6}$$

Substituting the parameters determined for different creep stresses at -10 ˚C, the axial strain rate can be obtained from (4.6). Furthermore, when integrating the axial strain rate such obtained, we can get the axial strain for different creep stresses. The changes

of the simulated axial strain and axial strain rate at -10 °C are presented in Figure 4.2 and 4.3, respectively. From these two figures we can see that: 1) the specimen experiences only the primary creep stage at low creep stress (*e.g.* 1000 and 3000 kPa), in which the creep strain will increase continuously with time, but the increase rate becomes lower and lower, as shown in Figure 4.3; 2) while at relatively high creep stress (*e.g.* 7000 and 8000 kPa), typical three-stage creep curve can be observed. In these tests, the creep strain increases continuously and the creep rate firstly decreases and then increases with an almost constant creep rate (steady-state) in between which can be seen clearly in a Cartesian coordinate system; and 3) at higher creep stress (*e.g.* 10 000 kPa), the creep strain increases sharply with time and the creep rate changes in a similar pattern to that at relatively high stress in the log-log coordinate system, but without the creep stage of constant rate in the Cartesian coordinate system, *i.e.* the primary creep stage is followed closely by the tertiary creep stage. Comparison between the experimental and numerical results in Figures 4.2 and 4.3 shows that the above variation patterns of creep strain and creep rate can be well described by the hypoplastic creep model. Besides, it can be seen from Figure 4.3 that, in the case of failure, the time to creep failure decreases with creep stress, this can also be well captured by the model.

The hypoplastic creep model also shows a good ability in describing the effect of temperature on the creep behavior of frozen Karlsruhe medium sand. For the results of the compression creep tests at the temperature of -2 °C, the simulation procedures are analogous to that at the temperature of -10 °C. The simulated results are shown in Figures 4.4 and 4.5, which can be regarded as a further validation of the creep model. Based on Figures 4.2-4.5, the effect of temperature on the creep behavior of frozen sand can be summarized as: 1) the strength properties of the frozen sand are enhanced when the temperature decreases, *i.e.* higher stress is required for the creep failure at lower temperature; 2) the steady-state creep stage is shortened as the temperature decreases, see Figures 4.2 and 4.4. This implies that the mechanical behavior of frozen sand will change from a plastic type to a brittle type, which leads to 3) the creep rate after failure increases faster at lower temperature, see Figures 4.3 and 4.5.

Similar conclusions can also be found in the publications by Andersland and Akili (1967), Sayles (1968), Eckardt (1982) and Fish (1994).

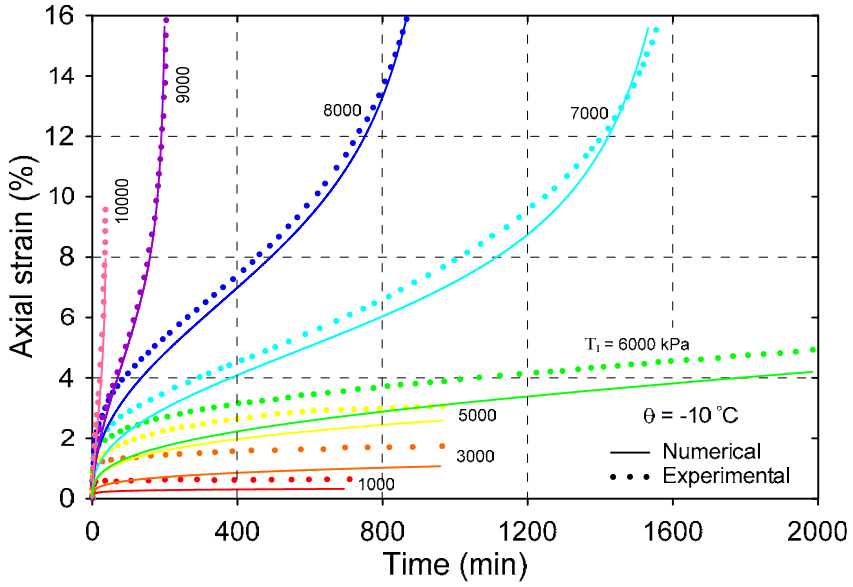

Fig. 4.2 Evolution of axial strain at different stress levels at -10 °C

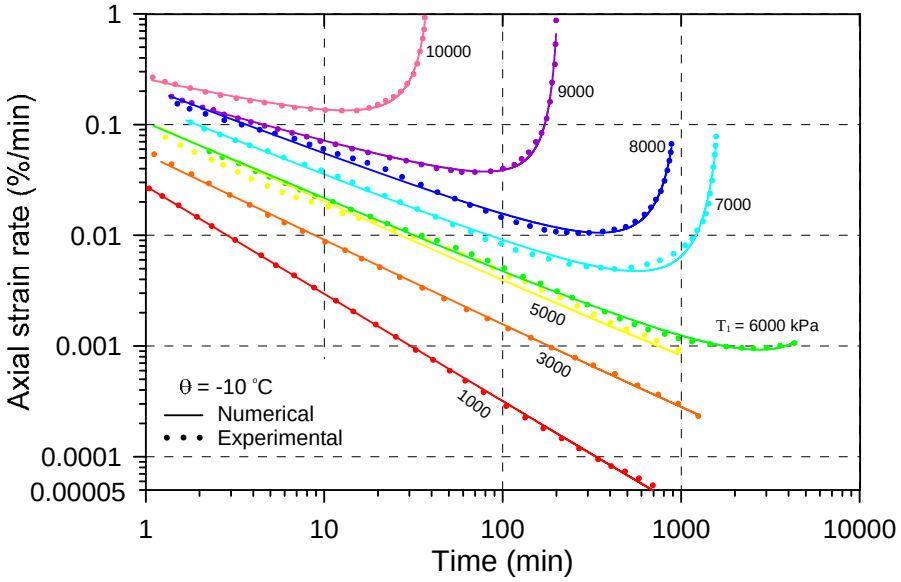

Fig. 4.3 Evolution of axial strain rate at different stress levels at -10 °C

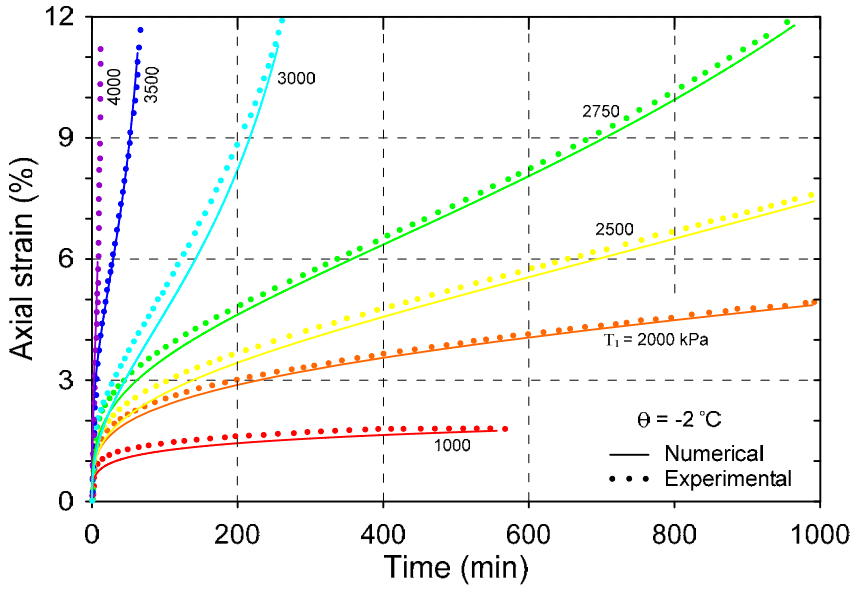

Fig. 4.4 Evolution of axial strain at different stress levels at -2 ˚C

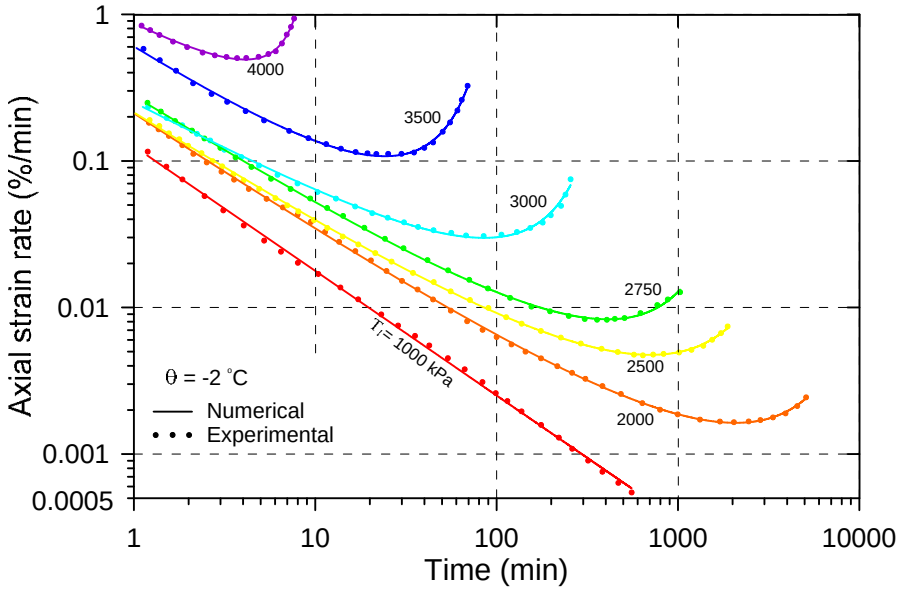

Fig. 4.5 Evolution of axial strain rate at different stress levels at -2 ˚C

4.3 Creep strength relaxation and steady creep rate

As is well known, frozen soils possess very strong rheological properties owing to the components of ice and unfrozen water, which will cause some prominent characteristics of frozen soils, such as long term deformation (creep), stress relaxation

and decrease of long term strength. If a creep process contains the tertiary creep stage, then creep failure can be defined as a point at which the tertiary creep stage begins, while for the case without the tertiary stage, certain creep strain, *e.g.* 20%, is often taken as the failure criterion. Many creep test results (Rein *et al*., 1975; Orth, 1986; Wu and Ma, 1994) show that the time to failure changes a lot when different creep stresses are used in creep tests, in turn we can say, the strength of frozen soil in creep tests will change with the time to failure. For example, when frozen soil fails in a short period of time, the creep strength will be relatively high (the stress leading to such a quick failure of frozen soil is regarded as the instantaneous strength), with the increase of the time to failure, the creep strength will continuously decrease to a series of long-term strengths, and then tend towards a constant value, which is often referred to as ultimate of long-term strength. Hence, when plotting the creep strength of frozen soil against the corresponding time to failure, a relaxation curve can be obtained.

The relaxation curve of the creep strength of frozen Karlsruhe medium sand is presented in Figure 4.6, from which we can see clearly that the creep strength decreases continuously with time from the instantaneous strength to the ultimate of long-term strength. The whole relaxation process can be divided into 3 stages, namely strong relaxation stage, slight relaxation stage and relatively steady stage. Corresponding to each stage, the magnitude of the relaxation rate will decrease fast, slow and then asymptotically approach 0. Based on the hypoplastic creep model presented in Section 4.1, a unified relaxation equation for the creep strength of frozen Karlsruhe medium sand can be obtained as

$$\log t_{\mathrm{f}} = \sqrt{\frac{b}{a}} - d \tag{4.7}$$

in which t_{f} is the time to failure, a, b and d are parameters dependent on creep stress at a certain temperature, as talked in (4.2). It can be easily known from (4.7) that the creep strength is related to the time to failure by a logarithmic function. By comparing the results calculated with (4.7) to the experimental data on creep strength, as shown in Figure 4.6, we can find that the relaxation equation is capable of describing the decrease of creep strength of frozen Karlsruhe medium sand over a certain time range.

Similar relaxation equations were also proposed by Vyalov (1962) for frozen soils, and by Brostow *et al*. (1993) for metals and polymers.

As temperature is the crucial influence factor on the mechanical properties of frozen soil, the temperature effect on the relaxation of creep strength is also presented in Figure 4.6. It can be seen from Figure 4.6 that, at the same time to failure, the creep strength will increase with the decrease of temperature from -2 to -10 °C. Besides, temperature decrease will lead the mechanical behavior of frozen soil to a brittle type from a plastic type. Therefore the relatively steady stage in the relaxation process will be delayed at lower temperature, as shown in Figure 4.7, the relaxation rate of creep strength at -2 °C approaches 0 earlier than that at -10 °C. Such conclusions are also obtained by Wu and Ma (1994) in the tests on frozen calcareous clay over a broader temperature range from -2 to -15 °C.

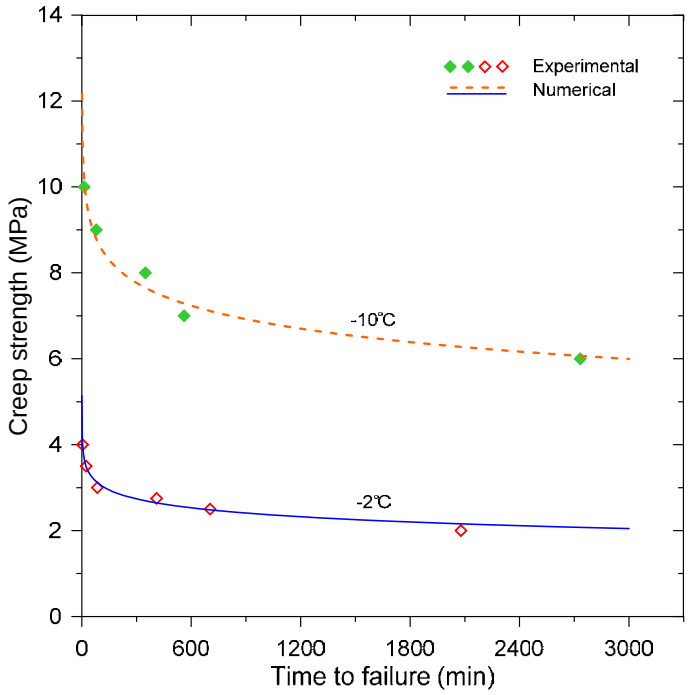

Fig. 4.6 Relaxation of the creep strength of frozen Karlsruhe Medium sand

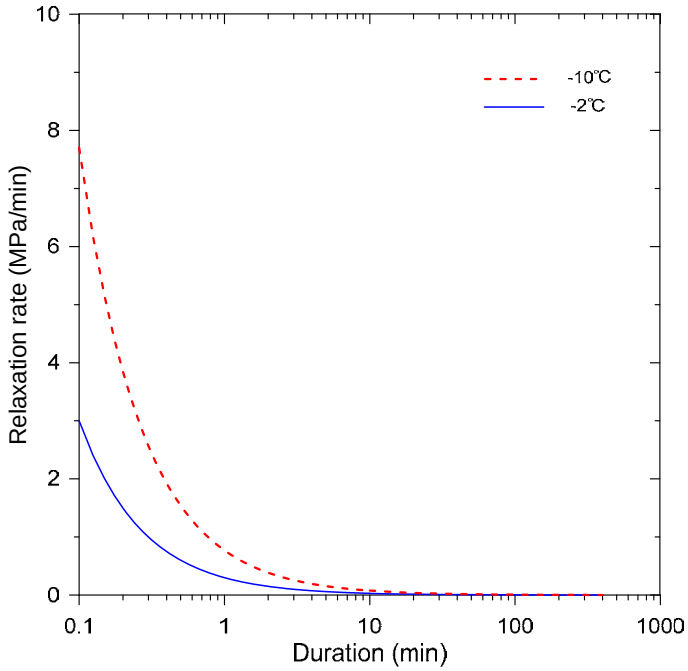

Fig. 4.7 Relaxation rate of the creep strength at different temperatures

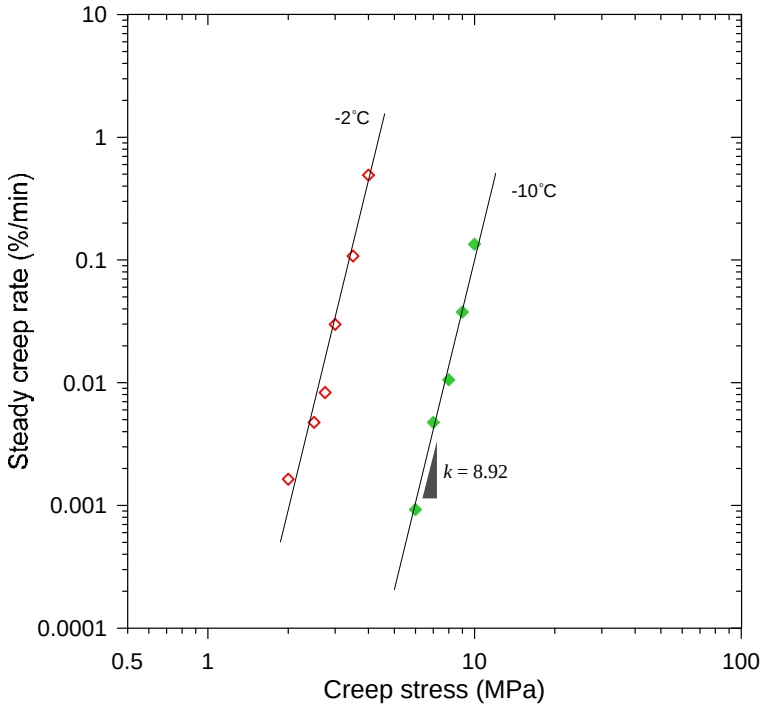

Fig. 4.8 Steady-state creep rate vs. creep stress at different temperatures

As talked in Subsection 3.2.2, the creep rate in the secondary creep stage changes very little in a linear Cartesian coordinate system, thus the secondary creep stage is often regarded as a steady-state creep stage, and the creep rate in this stage can be referred to as steady flow rate (Ting, 1983; Wu and Ma, 1994). Many creep test

results (Ladanyi, 1972; Mellor and Cole, 1982; Ting, 1983) indicate that the steady flow rate hinges on the creep stress level. If the creep stress is less than the ultimate of long-term creep strength, the steady flow rate will tend towards 0; while the creep stress is greater than the ultimate, the flow rate will increase with the difference between the creep stress and the ultimate strength, *i.e.* $T - T_u$. Hence, when the steady-state creep stage is dominant in the whole creep process, it will be significative to study the steady flow rate, for which would play an important role in developing a secondary creep model.

The change of the steady flow rate of frozen Karlsruhe medium sand with creep stress is presented in the log-log plot in Figure 4.8, from which an approximately linear relationship can be observed, and the slopes of the lines for different temperatures change not so much and have an average of 8.92. Assuming that the relationship between the steady flow rate and the creep stress can be described by a power function, then the exponent of the power function will be identical with the slope of the lines. Similar results were also reported by Thompson and Sayles (1972) on frozen Fairbanks silt with a slope of 4.0 and by Ting (1983) on frozen Manchester fine sand with an average slope of 9.88.

5 Conclusion and discussion

Three constitutive models are developed for frozen soils in this study based on the hypoplastic constitutive model proposed by Wu (1992) for sand. The commonality of the three models is that a cohesion tensor is introduced to account for the tensile properties of frozen soils. In this ending section, the main conclusions of this study will be listed in the first part, followed by some open questions about each model in the second part.

5.1 Main work and conclusions

The main work and conclusions of this study can be summarized as

(1) By introducing a cohesion tensor and a scalar function related to deformation into the model by Wu (1992), an extended hypoplastic constitutive model is proposed for frozen soil, as shown in Section 2. Simulation results indicate that this model is capable of describing the effects of temperature and confining pressure on the mechanical properties of frozen soils. These are realized by the linear dependence of the cohesion tensor on temperature and its inherent stress-dependence of the proposed model. It should be noted that this model is rate-independent, therefore cannot take into account the rheological properties of frozen soil.

(2) Based on the rate-independent hypoplastic constitutive model in Section 2, a rate-dependent hypoplastic constitutive model, named as visco-hypoplastic constitutive model, is developed in Section 3 to account for the rheological behaviors, such as rate effect and creep behavior, of frozen soils. This viscous model is obtained by dividing the stress rate into a statical and a dynamical part, which are represented by the rate-independent model in Section 2 and a high order model with the term of strain acceleration, respectively. Then the versatility of the viscous model is verified by simulating some compression tests at different loading rates and some creep tests at different creep stresses. Hence, such model could be used to evaluate the effect of construction/excavation rate on the

stability of structures in frozen ground engineering. It can be further noted that the viscous model can describe the complete three-stage creep process in a unified way, rather than simulating each creep stage separately as done by secondary or tertiary creep models.

(3) Another rate-dependent hypoplastic constitutive model, termed hypoplastic creep model, is developed in Section 4. The model parameters, which can be determined from a creep rate curve with the tertiary creep stage, are found to have a linear relationship with the creep stress, regardless of failure occurs or not. By simulating some compression creep tests at different temperatures and creep stresses, the hypoplastic creep model shows a good ability in describing the creep behaviors of frozen soil, *e.g.* the time to creep failure and the minimum creep rate in the steady-state creep stage. Besides, the relaxation of creep strength of frozen soil can also be described by this creep model, which will help to evaluate the service life of structures in permafrost regions.

5.2 Open questions and discussion

Although several constitutive models have been developed for frozen soils in this study, there are still some problems worthy of attention and need to be declared, such as the limitation of the models, feasible extension or reasonable improvement to the models. These problems are presented in below.

(1) The three constitutive models for frozen soils in this study are isotropic, but in general, the natural frozen soils are anisotropic or transverse isotropic. Therefore, anisotropic constitutive models could be considered as a research target in the future work.

(2) As is known to all, the strength of granular materials, *e.g.* soil, will be enhanced when the stress level increases. However, this is not always correct for frozen soil. Specifically, at a relatively low stress range, the strength of frozen soil will increase with stress level. With the further increase of stress level, the strength of

frozen soil will decrease, as the ice in the intergranular pores will melt owing to the high stress (Chamberlain *et al*., 1972; Parameswaran and Jones, 1981; Ma *et al*., 1995). Such peculiar phenomenon cannot be described by the models in this study. Therefore, special efforts may still be needed for modeling frozen soils under high stress.

(3) In the simulation of the triaxial compression tests on frozen silt in Section 2, small discrepancy occurs in the description of volumetric deformation. The reason for this may lie in: homogeneous deformation is assumed throughout the simulation in which the specimen is regarded as one element, while in the laboratory test, the main deformation will concentrate within the shear bands in the specimen after a short period of homogeneous deformation. In view of this, an extension of the hypoplastic constitutive model in Section 2 may be taken into account in order to perform a multi-scale analysis of the specimen.

(4) The visco-hypoplastic constitutive model in Section 3 has been proved to have a good performance, it can describe not only creep tests at different stresses, but also compression tests at different loading rates. However, the calibration of the model is a challenge. In the simulations in Section 3, the model parameters are obtained by fitting experimental data. Hence, some effective methods for determining the parameters are still in need.

(5) The visco-hypoplastic constitutive model, owing to the existence of a high order term of strain, cannot be implemented into the conventional numerical methods in geotechnical engineering, such as the finite element method and finite difference method. However, recalling the process of developing the viscous model, see Section 3.1, we can know that the high order part has an origin from fluid mechanics. Hence, instead of the conventional numerical methods, a promising alternative will be the Particle-in-Cell method, for which is relatively intuitive and straightforward to implement and could also be applied to problems on fluid and granular materials (Harlow *et al*., 1964; Cummins and Brackbill, 2002), in addition to plasma physics.

Bibliography

1. Andersland O.B. and Akili W.: Stress effect on creep rates of a frozen clay soil. Geotechnique, 1967, 17: 27 - 39.
2. Assur A.: Some Promising Trends in Ice Mechanics. In Physics and Mechanics of Ice. International symposium, Copenhagen, 1980, 1 - 15.
3. Bagnold R. A.: Experiments on a Gravity-Free Dispersion of Large Solid Spheres in a Newtonian Fluid under Shear. Proceedings of the Royal Society of London. Series A. Mathematical and Physical Sciences, 1954, 225(1160): 49 - 63.
4. Bauer E., Wu W.: A hypoplastic constitutive model for cohesive powders. Powder Technology, 1995, 85: 1 - 9.
5. Bourbonnais J., Ladanyi B.: The mechanical behavior of frozen sand down to cryogenic temperatures. Proceedings of the 4th International Symposium on Ground Freezing, Sapporo, Japan, 1985, 1: 235 - 244.
6. Bragg R.A., Andersland O.B.: Strain rate, temperature, and sample size effects on compression and tensile properties of frozen soil. Engineering Geology, 1981, 18: 35 - 46.
7. Brostow W., Kubat J., Kubat M. J.: Stress Relaxation In Metals And Polymers: Theory, Experiment And Computer Simulations. Materials Research Society Symposium Proceedings, 1993, 321: 99 - 106.
8. Cai Z., Zhu Y., Zhang C.: Viscoelastoplastic constitutive model of frozen soil and determination of its parameters. Journal of Glaciology and Geocryology, 1990, 12(1): 31 - 40.
9. Chamberlain E., Groves C., Perham R.: The mechanical behavior of frozen earth materials under high pressure triaxial test conditions. Journal of Geotechnical, 1972, 22(3): 469 - 483.
10. Cummins S.J., Brackbill J.U.: An Implicit Particle-in-Cell Method for Granular

Materials. Journal of Computational Physics, 2002, 180(2): 506 - 548.

11. Dafalias Y. F.: Bounding surface plasticity, I: Mathematical foundation and hypoplasticity. ASCE Journal of Engineering Mechanics, 1986, 112(9): 966 - 987.
12. Eckardt H.: Creep tests with frozen soils under uniaxial tension and uniaxial compression. Proceedings of the 4th Canadian Permafrost Conference, 1982, 394 - 405.
13. Fish A.M.: Comparative analysis of the USSR construction codes and the US Army technical manual for design of foundations on permafrost. US Army, Cold Regions Research and Engineering Laboratory (CRREL), 1982, Report 82-14, p. 20.
14. Fish A.M.: Creep and Strength of Frozen Soil Under Triaxial Compression. U. S. Army Cold Regions Research and Engineering Laboratory, technical report.1994.
15. Fröhlich H., Sack R.: Theory of the rheological properties of dispersions. Proc. Roy. Soc. 1946, A185: 415 - 430.
16. Goldhirsch I., Sela N.: Origin of normal stress differences in rapid granular flows. Phys. Rev. E 1996, 54: 4458 - 4461.
17. Goldscheider M.: True triaxial tests on dense sand. Results of the Int. Workshop on Constitutive Relations for Soils, Balkema, Rotterdam, the Netherlands, 1982, 11 - 54.
18. Goodman M. A., Cowin S. C.: Two problems in the gravity flow of granular materials. Journal of Fluid Mechanics, 1971, 45: 321 - 339.
19. Goodman M.A., Cowin S.C.: A continuum theory for granular materials. Archive for Rational Mechanics and Analysis, 1972, 44(4): 249 - 266.
20. Goughnour R.R., Andersland O.B.: Mechanical Properties of A Sand-Ice System. Journal of soil mechanics and foundation division, ASCE, 1968, 94(4): 923 - 950.
21. Hanes D. M., Inman D. L.: Observations of rapidly flowing granular-fluid materials. Journal of Fluid Mechanics, 1985, 150: 357 - 380.
22. Harlow F. H., Ellison M. A., Reid J. H.: The Particle-in-Cell Computing Method for Fluid Dynamics. Methods of Computational Physics, 1964, 3(3): 319 - 343.

23. Haynes F.D., Karalius J.A.: Effect of temperature on the strength of frozen silt. USA CRREL Report 77-3, 1977.
24. He P., Cheng G.D., Zhu Y.L.: Constitutive theories on viscoelstoplasticity and damage of frozen soil. Science in China (D), 1999, 42: 38 - 43.
25. Herle I., Kolymbas D.: Hypoplasticity for soils with low friction angles. Computers and Geotechnics, 2004, 31: 365 - 373.
26. Huang W.X., Wu W., Sun D.A., Sloan S.: A simple hypoplastic model for normally consolidated clay. Acta Geotechnica, 2006, 1: 15 - 27.
27. Hult J. A. H. (1966) Creep in engineering structures. Blaisdell Publ. Co., Waltham, Mass. pp.115.
28. Kolymbas D.: A generalized hypoplastic constitutive law. Proceedings of the 11th Int. Conf. SMFE, 1985.
29. Kumagai N., Sasajima S., Ito H.: Long-term Creep of Rocks: Results with Large Specimens Obtained in about 20 Years and Those with Small Specimens in about 3 Years. Journal of the Society of Materials Science, 1978, 27(293): 155 - 161.
30. Ladanyi B.: An engineering theory of creep of frozen soils. Canadian Geotech. J. 1972, 9(1): 63 - 80.
31. Ladanyi B.: Mechanical behaviour of frozen soils. Proc. Int. Symp. on Mechanical Behavior of Structured Media, Carleton Univ., Ottawa. New York: 1981, B: 205 - 245.
32. Lai Y.M., Jin L., Chang X.X.: Yield criterion and elasto-plastic damage constitutive model for frozen sandy soil. International Journal of Plasticity, 2009, 25: 1177 - 1205.
33. Li G.: Advanced soil mechanics. Tsinghua University Press, 2004.
34. Li H.S., Yang, H.T., Chang C., Sun X.T.: The strain rate sensitivity analysis of compression strength of frozen soil. Journal of Glaciology and Geocryology, 1995, 17(1): 40 - 48.
35. Ma W., Wu Z.W., Sheng Y.: Effect of Confining Pressure on Strength Behaviour of Frozen Soil. Chinese Journal of Geotechnical Engineering, 1995, 17(5): 7 - 11.
36. Massoudi M., Boyle E.J.: A Review of Theories for Flowing Granular Materials

with Applications to Fluidized Beds and Solids Transport. USDOE Pittsburgh Energy Technology Center, 1991.

37. Maxwell J. C.: On the Dynamical Theory of Gases. Philosophical Transactions of the Royal Society of London, 1867, 157: 49 - 88.
38. Meissner J., Garbella R. W., Hostettler J.: Measuring Normal Stress Differences in Polymer Melt Shear Flow. Journal of Rheology, 1989, 33(6): 843 - 864.
39. Mellor M., Cole D.M.: Deformation and failure of ice under constant stress or constant strain-rate. Cold Regions Science and Technology, 1982, 5: 201 - 219.
40. Ning J.G., Zhu Z.W.: Constitutive model of frozen soil with damage and numerical simulation of the coupled problem. Chinese Journal of Theoretical and Applied Mechanics, 2007, 39(1): 70 - 76.
41. Nunziato J. W., Passman S. L., Thomas J. P.: Gravitational Flows of Granular Materials with Incompressible Grains. Journal of Rheology, 1980, 24(4): 395 - 420.
42. Okubo S., Nishimatsu Y., Fukui K.: Complete creep curves under uniaxial compression. International Journal of Rock Mechanics and Mining Sciences and Geomechanics Abstracts, 1991, 28(1): 77 - 82.
43. Orth W.: Gefrorener Sand als Werkstoff: Elementversuche und Materialmodell. Publication Series of the Institute of Soil Mechanics and Rock Mechanics, Karlsruhe University, No. 100, 1986.
44. Parameswaran V.R.: Deformation behaviour and strength of frozen sand. Canadian Geotechnical Journal, 1980, 17(1): 74 - 88.
45. Parameswaran V.R., Jones S.J.: Triaxial testing of frozen sand. Journal of Glaciology, 1981, 27(95): 147 - 156.
46. Passman S.L., Thomas J. P., Bailey P. B., Nunziato J. W.: Shearing Flows of Granular Materials. Journal of the Engineering Mechanics Division, 1980, 106(4): 773 - 783.
47. Phan-Thien, Nhan: Understanding Viscoelasticity: Basics of Rheology. 2002.
48. Qi J.L., Sheng Y., Zhang J.M., Wen Z.: Settlement of embankments in permafrost regions in theQinghai-Tibetan plateau. Norw. J. Geogr., 2007, 61: 49 - 55.

49. Rein R. G., Hathi V. V., Sliepcevich C. M.: Creep of sand-ice system. ASCE Journal of the Geotechnical Engineering Division, 1975, 101(GT2): 115 - 128.
50. Rivlin R.S., Ericksen J.L.: Stress-Deformation Relations for Isotropic Materials. Jouranl of Rational Mechanics and Analysis, 1955, 4: 323 - 425.
51. Rong C.X., Wang X.X., Cheng H.: An experimental study on finite strain constitutive relations of frozen soil. Journal of experimental mechanics, 2005, 20(1): 133 - 138.
52. Savage S. B.: Gravity flow of cohesionless granular materials in chutes and channels. Journal of Fluid Mechanics, 1979, 92: 53 - 96.
53. Savage S. B., Mckeown S.: Shear stresses developed during rapid shear of concentrated suspensions of large spherical particles between concentric cylinders. Journal of Fluid Mechanics, 1983, 127: 453 - 472.
54. Sayles F.H.: Low Temperature Soil Mechanics. U.S. Army Cold Regions Research and Engineering Laboratory, Technical Note, Sep. 1966.
55. Sayles F.H.: Creep of frozen sands. U. S. Army Cold Regions Research and Engineering Laboratory, Technical Report 190, 1968, 47 - 48.
56. Scheiwiller T., Hutter K.: Übersicht über Experimente und theoretische Modelle von Fliess- und Staublawinen" ETH Press, 1982.
57. Stetzler-Kaufmann B.: Stoffverhalten chemisch injizierter Sande. Institut für Bodenmechanik und Felsmechanik der Universität Fridericiana, 1983.
58. Thompson E. G., Sayles F. H.: In situ creep analysis of room in frozen soil. ASCE Journal of the soil mechanics and foundation division, 1972, 98(SM9): 899 - 915.
59. Ting J.M.: Tertiary creep model for frozen sands. J. Geotech. Geoenviron. Eng., 1983, 109(7): 932 - 945.
60. Truesdell C.: Hypo-elasticity. Journal of Rational Mechanics Analysis, 1955, 4: 83 - 133.
61. Truesdell C., Noll W.: The Non-linear Field Theories of Mechanics. Handbuch der Physik, b. III/3, Berlin-Heidelberg-New York: Springer, 1965.
62. Vyalov S. S.: The strength and creep of frozen soils and calculations for ice-soil

retaining structures. U.S. Army CRREL, Translation 76, 1965.

63. Vyalov S. S.: Rheological Principles of Soil Mechanics. (in Chinese) Higher Education Press, Beijing, 1978.
64. Vyalov, S. S.: Rheological Properties and Bearing Capacity of Frozen Soils. U. S. Army Cold Regions Research and Engineering Laboratory, technical report, 1962.
65. Wang C.C.: A new representation theorem for isotropic functions, parts I and II. Journal of Rational Mechanics Analysis, 1970, 36: 166 - 223.
66. Wu W.: Hypoplasticity as a mathematical model for the mechanical behavior of granular materials. Publication Series of the Institute of Soil Mechanics and Rock Mechanics, Karlsruhe University, No. 129, 1992.
67. Wu W.: On High-order Hypoplastic Models for Granular Materials. Journal of Engineering Mathematics, 2006, 56(1): 23 - 34.
68. Wu W., Bauer E.: A simple hypoplastic constitutive model for sand. International Journal for Numerical and Analytical Methods in Geomechanics, 1994, 18(12): 833 - 862.
69. Wu W., Bauer E., Kolymbas D.: Hypoplastic constitutive model with critical state for granular materials. Mechanics of Materials, 1996, 23: 45 - 69.
70. Wu W., Bauer E., Niemunis A., Herle I.: Visco-Hypoplastic Models for Cohesive Soils. Modern Approaches to Plasticity, 1993: 365 - 383
71. Wu W., Kolymbas D.: Numerical testing of the stability criterion for hypoplastic constitutive equations. Mechanics of Materials, 1990, 9(4): 245 - 253.
72. Wu Z.W., Ma W.: Strength and Creep of Frozen Soil. Lanzhou University Press, 1994.
73. Zhang C.Q., Wei X.X., Miao T.D.: Microstructure Damage Behaviour and Change Characteristic in the Frozen Soil Creep Process. Journal of Glaciology and Geocryology, 1995, 17: 60 - 65.
74. Zhang G., Zhang J.M., Wu W.: A hypoplastic model of gravelly soil considering physical state. Chinese Journal of Rock and Soil Mechanics, 2008, 29(6): 1530 - 1534.

75. Zhu Y.L., Carbee D.L.: Creep behavior of frozen silt under constant uniaxial stress. Proc., 4th Int. Conf. on Permafrost, Fairbanks, Alaska, 1983, 1507 - 1512.
76. Zhu Y.L., Carbee D.L.: Uniaxial compressive strength of frozen silt under constant deformation rates. Cold Regions Science and Technology, 1984, 9: 3 - 15.